Neurobiology of Disease 88 (2016) 125–138

Contents lists available at ScienceDirect

Neurobiology of Disease

journal homepage: www.elsevier.com/locate/ynbdi

Impaired cognitive discrimination and discoordination of coupled theta–gamma oscillations in Fmr1 knockout mice

Basma Radwan [a,1], Dino Dvorak [a,b,1], André A. Fenton [a,c,*]

[a] Center for Neural Science, New York University, USA
[b] Joint Graduate Program in Biomedical Engineering State University of New York, Downstate Medical Center and New York University/Polytechnic University, USA
[c] Department of Physiology and Pharmacology, The Robert F. Furchgott Center for Neural & Behavioral Science, State University of New York, Downstate Medical Center, Brooklyn, NY, USA

ARTICLE INFO

Article history:
Received 3 November 2015
Revised 31 December 2015
Accepted 7 January 2016
Available online 12 January 2016

Keywords:
Fragile X
Neural coordination
Cross-frequency coupling
Phase–amplitude coupling
Theta–gamma comodulation
Spatial cognition

ABSTRACT

Fragile X syndrome (FXS) patients do not make the fragile X mental retardation protein (FMRP). The absence of FMRP causes dysregulated translation, abnormal synaptic plasticity and the most common form of inherited intellectual disability. But FMRP loss has minimal effects on memory itself, making it difficult to understand why the absence of FMRP impairs memory discrimination and increases risk of autistic symptoms in patients, such as exaggerated responses to environmental changes. While Fmr1 knockout (KO) and wild-type (WT) mice perform cognitive discrimination tasks, we find abnormal patterns of coupling between theta and gamma oscillations in perisomatic and dendritic hippocampal CA1 local field potentials of the KO. Perisomatic CA1 theta–gamma phase–amplitude coupling (PAC) decreases with familiarity in both the WT and KO, but activating an invisible shock zone, subsequently changing its location, or turning it off, changes the pattern of oscillatory events in the LFPs recorded along the somato-dendritic axis of CA1. The cognition-dependent changes of this pattern of neural activity are relatively constrained in WT mice compared to KO mice, which exhibit abnormally weak changes during the cognitive challenge caused by changing the location of the shock zone and exaggerated patterns of change when the shock zone is turned off. Such pathophysiology might explain how dysregulated translation leads to intellectual disability in FXS. These findings demonstrate major functional abnormalities after the loss of FMRP in the dynamics of neural oscillations and that these impairments would be difficult to detect by steady-state measurements with the subject at rest or in steady conditions.

1. Introduction

Cognitive discriminations require distinguishing between similar but distinct experiences. Since multiple experiences are always serial, at least one must be represented in memory. Such discriminations require the coordinated temporal binding and segregation of neural representations in the ongoing electrical activity within and between networks of neurons (Phillips and Singer, 1997; Johnson and Redish, 2007; Lisman and Buzsaki, 2008; Buzsaki, 2010; Kelemen and Fenton, 2010; Kelemen and Fenton, 2013).

Cognitive discriminations are impaired in Fragile X Syndrome (FXS) patients (Bailey et al., 1998; Holsen et al., 2008; Hooper et al., 2008; Ornstein et al., 2008), which may result in both impaired learning and exaggerated responding to small alterations of the environment. FXS is caused by silencing of the FMR1 gene (Pieretti et al., 1991; Colak et al., 2014) and the consequent failure to make the fragile X mental retardation protein (FMRP) that participates in RNA metabolism (Jin et al., 2004; Park et al., 2008; Kao et al., 2010; Melko and Bardoni, 2010). Despite detailed molecular knowledge of the role of FMRP and the consequences of its absence, the systems-level knowledge is inadequate and how dysregulated translation results in cognitive dysfunction is unknown.

Loss of FMRP in mouse models is associated with alterations in synaptic development and function (Comery et al., 1997; Braun and Segal, 2000; Bassell and Warren, 2008). Cognitive discrimination deficits are prominent in Fmr1 knockout (KO) rodents that do not make FMRP, although learning and memory per se are relatively normal (Bakker et al., 1994; D'Hooge et al., 1997; Zhao et al., 2005; Brennan et al., 2006; Bhattacharya et al., 2012; Till et al., 2015). Indeed, loss of FMRP did not alter activity-dependent synaptic plasticity in cultured neurons (Segal et al., 2003) but is associated with enhanced mGluR-stimulated hippocampal long-term depression (LTD) (Huber et al., 2002). While altered hippocampal long-term potentiation (LTP) is not typical in Fmr1 KO mice (Godfraind et al., 1996), when it is observed the deficit is in LTP stability (Lauterborn et al., 2007). Reduced or abolished LTP is observed in neocortex and amygdala (Larson et al., 2005; Zhao et al., 2005; Shang et al., 2009; Chen et al., 2014). However, the functional changes that link dysregulated translation to impaired cognition are unknown, and a theory is lacking.

* Corresponding author at: Neurobiology of Cognition Laboratory, Center for Neural Science, New York University, 4 Washington Place, NYC, NY 10012, USA.
[1] These authors made equal contributions to this work.
Available online on ScienceDirect (www.sciencedirect.com).

http://dx.doi.org/10.1016/j.nbd.2016.01.003
0969-9961/

In spatially layered structures like hippocampus (Fig. 1A, B), oscillations in the local field potential (LFP) arise from locally synchronous activation of synaptic currents. When filtered for the major oscillatory bands such as theta (5–12 Hz) and gamma (30–100 Hz; Fig. 1C), these local events appear synchronized across layers but upon closer inspection there are also significant deviations from global synchrony that are localized in both time and space (Fig. 1D). These local oscillatory variations reflect significant local variations in synaptic activity and representational information, as demonstrated by decoding the current position of a freely-moving rat from local variations of theta oscillations (Agarwal et al., 2014). As illustrated in Fig. 1, while unitary theta and gamma oscillations can synchronize across layers of hippocampus (Fig. 1B), the coupling of theta and gamma oscillations is variably synchronized between layers because the nesting of local gamma oscillations within the concurrent theta oscillation can change abruptly and these changes can synchronize across specific hippocampal layers. The example LFPs from across dorsal hippocampus that are shown in Fig. 1D are all from within the same recording session. The two leftmost examples illustrate, respectively, independent and synchronized organization of gamma oscillations by theta phase between *stratum pyramidale* (sp) and adjacent *stratum radiatum* (sr). The two rightmost examples illustrate, respectively, independent and synchronized theta–gamma phase–amplitude organization between the molecular layer (DGm) and the suprapyramidal cell layer (DGs) of the dentate gyrus. The desynchronization and synchronization of such higher-order oscillatory phenomena and their potential to reflect cognition-dependent neural computations by synaptic activity (Colgin et al., 2009; Buzsaki, 2010) leads us to hypothesize that dysregulated translation in FXS is linked to impaired cognition by discoordinated oscillations of neuronal activity. This discoordination hypothesis reflects the fact that unitary processes can be intact, while their interactions are abnormal (Phillips and Silverstein, 2003; Lee et al., 2012; Lee et al., 2014; O'Reilly et al., 2014; Fenton, 2015). The discoordination hypothesis predicts relatively intact unitary neural oscillations such as theta due to rhythmic interneuron discharge (Buzsaki et al., 1983), and gamma oscillations due to GABAergic neurotransmission (Whittington et al., 1995; Csicsvari et al., 2003a; Whittington and Traub, 2003), but inappropriate interactions between neural oscillations such as the theta phase coupling of gamma oscillations illustrated in Fig. 1D (Bragin et al., 1995; Canolty et al., 2006; Tort et al., 2008), especially during cognitive discrimination challenges. According to this view, neural discoordination would alter computational processes and thus increase failures in cognitive discrimination and cognitive control that depend on the appropriate selection and suppression of neural representations of information (Fenton, 2008; Lisman and Buzsaki, 2008; Lee et al., 2012; Lee et al., 2014). Further, because the hypothesis predicts impaired interactions, this notion extends to spatial interactions, predicting that theta–gamma discoordination will be specific to particular recording sites such as the hippocampus CA1 *stratum pyramidale* (sp), *stratum radiatum* (sr), and *stratum lacunosum moleculare* (slm). The sr and slm sites receive distinct hippocampal CA3 and entorhinal cortical (EC) inputs, respectively (Fig. 1A). These inputs carry different kinds of spatial information that CA1 pyramidal cells must integrate and segregate, as appropriate for the specific cognitive requirements. CA3 principal cells are mainly place cells signaling location, whereas ECIII cells are grid cells, border and directional cells signaling conjunctions of distance, environmental borders, and direction information (O'Keefe and Burgess, 1996; Sargolini et al., 2006; Savelli et al., 2008; Zhang et al., 2013). Furthermore, it has been proposed that the CA3 → CA1 sr synapses are more associated with memory and expectations whereas the EC → CA1 slm synapses are associated with the current information that is to be encoded (Colgin et al., 2009; Fries, 2009; Bieri et al., 2014). According to this view, theta–gamma coupling of oscillations in the CA1 LFP will be necessary for the coordinated integration and segregation of neural activity and information when a subject is challenged to discriminate and selectively use memorized and current information. We tested these predictions by recording site-specific hippocampal LFPs and by estimating features of the theta–gamma phase amplitude coupling (Fig. 1E), as well as the phase synchrony of these oscillations between the input layers (Fig. 1F). These investigations were performed while WT and Fmr1 KO mice performed a rapidly learned, hippocampus- and LTP-dependent active place avoidance task with systematically varied demands for cognitive discrimination that are sufficient to persistently modify hippocampal neural network function (Cimadevilla et al., 2001; Pastalkova et al., 2006; Burghardt et al., 2012; Kheirbek et al., 2013; Park et al., 2015). Because we hypothesize these oscillatory phenomena reflect ongoing cognitive information processing, we did not assume that they are stationary across either the recording sites or the behavioral sessions, which varied in cognitive demand and experience.

2. Results

2.1. Cognitive discrimination is impaired in Fmr1 KO mice

We began by establishing that cognitive discrimination is impaired in Fmr1 KO mice using the active place avoidance paradigm (Fig. 2A) because, with this paradigm it is feasible to assess cognition-related neural coordination (Kelemen and Fenton, 2010; Lee et al., 2012; Kelemen and Fenton, 2013) while varying cognitive demand and holding the behavioral and sensory conditions effectively constant. Fmr1 KO mice were more active during pretraining (genotype × time, where time is the 10-min interval: effect of genotype: $F_{1,90} = 5.07$; $P = 0.03$), which is why the KO mice entered the equivalent location of a shock zone more than WT mice (Fig. 2B). There was a trend for active exploration, measured as distance traveled on the arena, to habituate in both genotypes (two-way genotype × time ANOVA; genotype: $F_{1,90} = 3.95$; $P = 0.05$; time $F_{2,90} = 2.52$; $P = 0.09$; interaction: $F_{2,90} = 0.08$; $P = 0.9$). When shock was turned on, the two genotypes could not be distinguished in their exploration as well as their ability to rapidly learn and remember to avoid shock (Fig. 2B; 3-way genotype × session × time ANOVA; genotype: $F_{1,276} = 3.71$; $P = 0.06$; session: $F_{2,276} = 27.53$; $P = 10^{-11}$; time: $F_{2,276} = 10.63$; $P = 10^{-5}$). Avoidance after a 24-h interval was also similarly strong between the genotypes during the retention session on Day 3 and the mice improved within the session (two-way genotype × time ANOVA; genotype: $F_{1,93} = 1.75$; $P = 0.2$; time $F_{2,93} = 6.26$; $P = 10^{-3}$). These observations establish that Fmr1 KO mice have similar motivation and ability to avoid shock, as well as equivalent spatial learning and long-term memory for the locations of shock.

Next we investigated cognitive discrimination by changing the location of shock. Note that this did not change the physical environment except during each 500-ms shock (Fig. 2C). Initially, both the WT and Fmr1 KO mice increased errors to a similar extent, indicating that both genotypes were challenged to ignore the initial location of shock and learn the new location of shock. However, with continued training, the WT mice rapidly learned to discriminate between the memories of the old and new shock locations, whereas the Fmr1 KO mice were slower to make the distinction (two-way genotype × time ANOVA; genotype: $F_{1,42} = 4.94$; $P = 0.03$; time: $F_{2,42} = 23.85$; $P = 10^{-7}$). We found no evidence of perseveration in the KO mice. For example, the ratio of time in the initial shock zone location versus the new shock zone was similar in the two genotypes during each 10-min period of the conflict session (genotype: $F_{1,41} = 0.001$; $P = 1$), and this ratio increased during the session (time: $F_{2,41} = 5.61$; $P = 0.007$). Unimpaired initial learning and memory confirm that basic information processing is intact in Fmr1 KO mice, whereas the conflict learning deficit demonstrates that cognitive discrimination is impaired but not because of perseveration.

We then tested the generality of the conclusion that cognitive discrimination is impaired in Fmr1 KO mice by making a different change

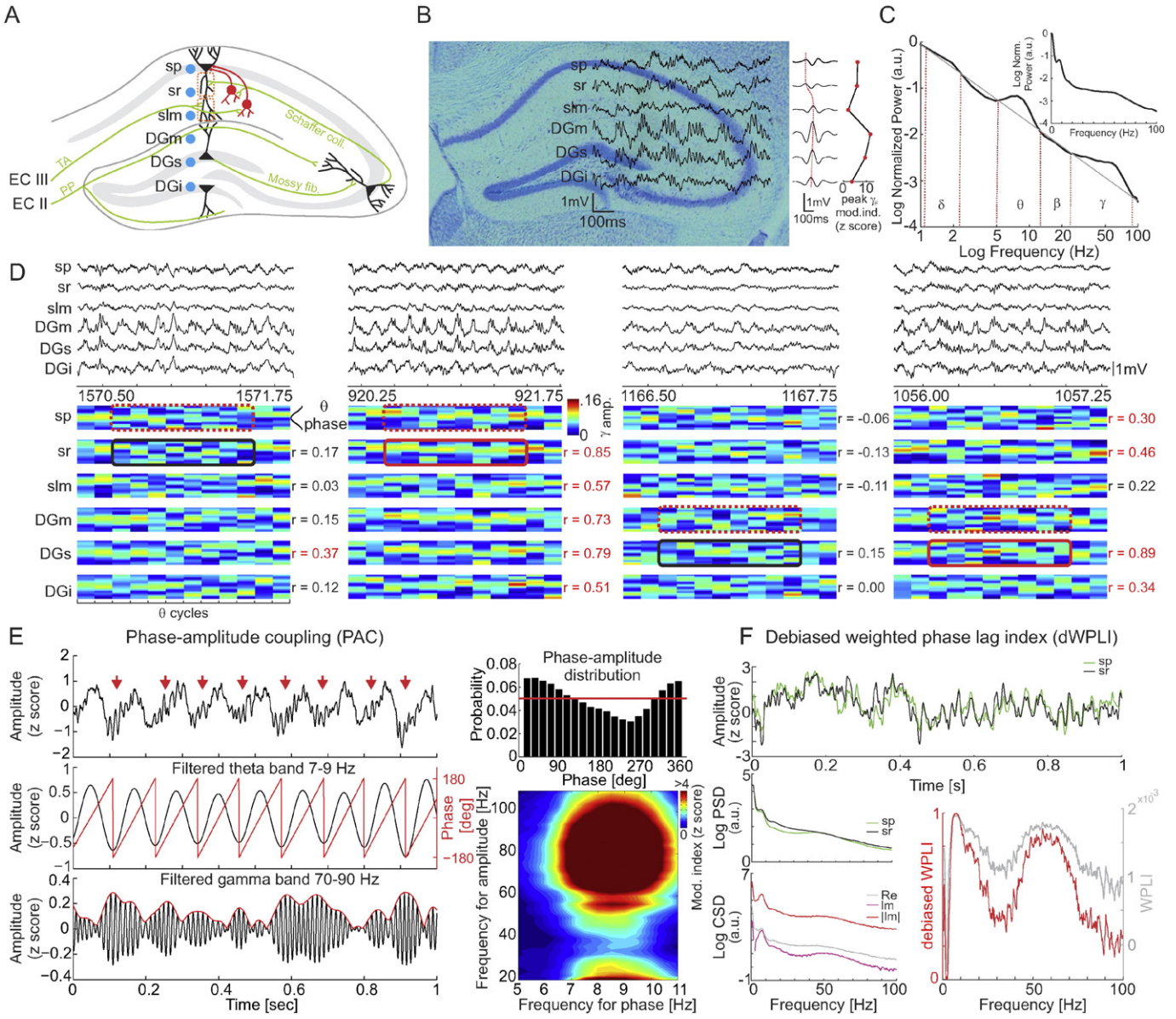

Fig. 1. Electrophysiology. (A) An electrode bundle with linear spacing was inserted along the CA1-DG axis to record local oscillatory activity from select domains of the hippocampal circuit. (B) A histological section with example LFP traces (left) and average LFP signals band-pass filtered in the theta band and time-locked to the strongest peaks of theta oscillations recorded from sp (middle). The red dotted line connects peaks across channels displaying the phase reversal between sr and slm used for identification of electrode locations. Profile of peak theta–fast gamma PAC across layers (right). (C) The average power spectra at sp from all mice during the pretraining session. The log–log plot shows that there are characteristic deviations from the 1/f power law, which define the frequency bands we analyzed. The inset shows the more familiar semi-log version of the power spectra. The theta (5–12 Hz) and gamma (30–90 Hz) bands are most prominent, followed by delta (1–3 Hz). Although it is not prominent in the hippocampal spectra, we also investigated the traditionally defined beta (20–30 Hz) band. (D) While theta and gamma oscillations often appear coherent across the layers, their interactions exhibit transient and abrupt, site-specific patterns of theta phase-gamma amplitude coupling. An example of this can be seen in the set of raw LFPs shown here. Below the traces are corresponding plots illustrating the color-coded theta phase-specific distribution of fast gamma oscillations during each theta cycle. These were computed by filtering the LFPs in the 7–12 Hz theta range and detecting their peaks. Fast gamma 60–90 Hz oscillation amplitudes were computed from the Hilbert transform after filtering. Phase distributions (18° bins) of gamma amplitudes were computed for each theta cycle defined by two consecutive theta peaks. The phase–amplitude histogram for each theta cycle was normalized by dividing by the histogram sum. Gamma amplitudes were extracted from all electrodes, but for these analyses, theta cycles were defined only by the sp signal to avoid differences between the electrodes caused by the theta phase reversal. Pearson's correlation was computed between the phase–amplitude histograms on the reference channel (sp or DGm) and the remaining channels. This example shows (far left) that theta–gamma coupling can be strongly synchronized at sp (dotted line, reference) with the DGs electrode and weakly synchronized with other sites, including the adjacent sr and slm sites, while at another instance (mid-left), theta–gamma coupling at sr can be strongly synchronized with the LFPs at all the recording sites. Similarly, theta–gamma coupling at DGm (dotted line, reference) can be effectively (mid-right) unrelated to theta–gamma coupling at the other electrode sites or (far-right) strongly correlated to many other electrode sites, but not only because the sites are adjacent. The correlation between the theta–gamma coupling profiles in the highlighted portions of the LFP are given, significant correlations are indicated in red. (E top, left) Phase–amplitude coupling (PAC) between theta and gamma rhythms can be identified visually in raw LFP traces. To quantify PAC (E middle, left) phase of the slow oscillation and (E bottom, left) amplitude of the fast oscillation are extracted and (E top, right) the phase–amplitude distribution is computed. The modulation index corresponds to a 'distance' between the resulting distribution and the uniform distribution (red line). Repeating the above steps for pairs of frequencies in the slow and fast frequency ranges results in (E bottom, right) a comodulogram. Modulation index values are normalized (z score) using surrogate series. (F) Phase synchrony between pairs of hippocampal LFPs (top) is estimated by computing the debiased weighted phase lag index (dWPLI). (left, middle) The power spectral density (PSD) from each voltage time series is computed (left bottom) followed by the real (Re) and imaginary (Im) components of the cross spectrum (CSD) and the absolute imaginary cross spectrum (|Im|). (right) WPLI and dWPLI estimates of phase synchrony are computed from the imaginary and absolute imaginary cross spectra according to Eqs. (1) and (2), respectively. The WPLI and dWPLI measures fail to estimate synchrony when phase differences are close to zero as in the case of delta oscillations, which is why delta phase synchrony was not computed.

to the location of shock. We reasoned that if mice received extinction training by turning off shock after the initial training phase, then by the end of the first extinction training session they would have two memories of being in the rotating arena — one memory with the shock being on and the other with the shock being off. Upon returning to the arena for a second extinction training session, the mice would be challenged to discriminate between the two memories and could either continue to avoid or continue to enter the former location of shock. In the first extinction session the WT and Fmr1 KO mice extinguished the avoidance at the same rate (two-way genotype × time ANOVA; genotype: $F_{1,45} = 1.77$; $P = 0.2$; time $F_{2,45} = 6.61$; $P = 0.003$; interaction: $F_{2,45} = 0.08$; $P = 0.92$; Fig. 2D). However, the genotypes differed on the second extinction session. Whereas WT mice continued to express an attenuated avoidance that was substantially better than chance, the KO mice initially behaved as if the avoidance was reinstated. As the session continued they rapidly extinguished the avoidance so that by the last 10 min they were performing at chance, having fully extinguished the conditioned avoidance (two-way genotype × time ANOVA; genotype: $F_{1,42} = 0.57$; $P = 0.5$; time $F_{2,42} = 4.56$; $P = 0.02$; interaction: $F_{2,42} = 3.96$; $P = 0.03$; Fig. 2D). We conclude that the cognitive discrimination deficit in Fmr1 KO mice is robust and can be observed in multiple ways using the place avoidance paradigm.

2.2. Minimal power spectral differences between Fmr1 KO and WT mice

We then examined the session- and site-specific power spectra for the two genotypes. After selecting epochs when the mice were moving (speed >3 cm/s) we find that spectral power at each electrode location was relatively unchanged across the training conditions (Fig. S1). In separate two-way genotype × session ANOVAs with repeated measures on the factor of sessions, the average power in the separate delta (1–3 Hz), theta (5–12 Hz), beta (20–30 Hz), and gamma (30–90 Hz) bands was compared across the pretraining, and three initial training sessions to evaluate the effect of learning to avoid the initial location of shock. Comparisons across the retraining and conflict sessions, and across the retraining and two extinction sessions were performed to evaluate the effects of cognitive discrimination on spectral power. Only two comparisons were significant. The effect of session on beta band power at slm was significant across initial learning because beta power on training trial 3 was greater than on the pretraining and first training trials. The second effect was across the extinction trials; the genotype × session interaction was significant at the DGi electrode in the beta band but no pairwise differences reached significance. Thus spectral power across the hippocampus was rather insensitive to the cognitive and genotypic status of the WT and Fmr1 KO mice.

2.3. Weak theta–gamma phase–amplitude coupling abnormalities in stratum pyramidale of Fmr1 KO mice

We investigated whether the Fmr1 KO mice express cognition-related aberrations in the neural coordination of oscillations and whether these are most prominent during the conflict and extinction training sessions, when cognitive discrimination deficits were observed. The average session- and electrode-specific comodulograms for each genotype, are shown for the full set of electrode locations in Fig. S2, whereas Fig. 3A shows the data subset for the LFPs at *stratum pyramidale*. There is a single prominent blob indicating significant phase-amplitude coupling (PAC) between ~8 Hz (theta) and 60–80 Hz (fast gamma). We did not observe a separate PAC peak in the 25–50 Hz slow gamma band except in the mutants at the deepest electrodes in the dentate gyrus (Fig. S2A, Fig. S3). We also observed theta-modulated high frequency (140–150 Hz) oscillations (HFO) in *stratum oriens-alveus* (Patel et al., 2012; Eadie et al., 2012),

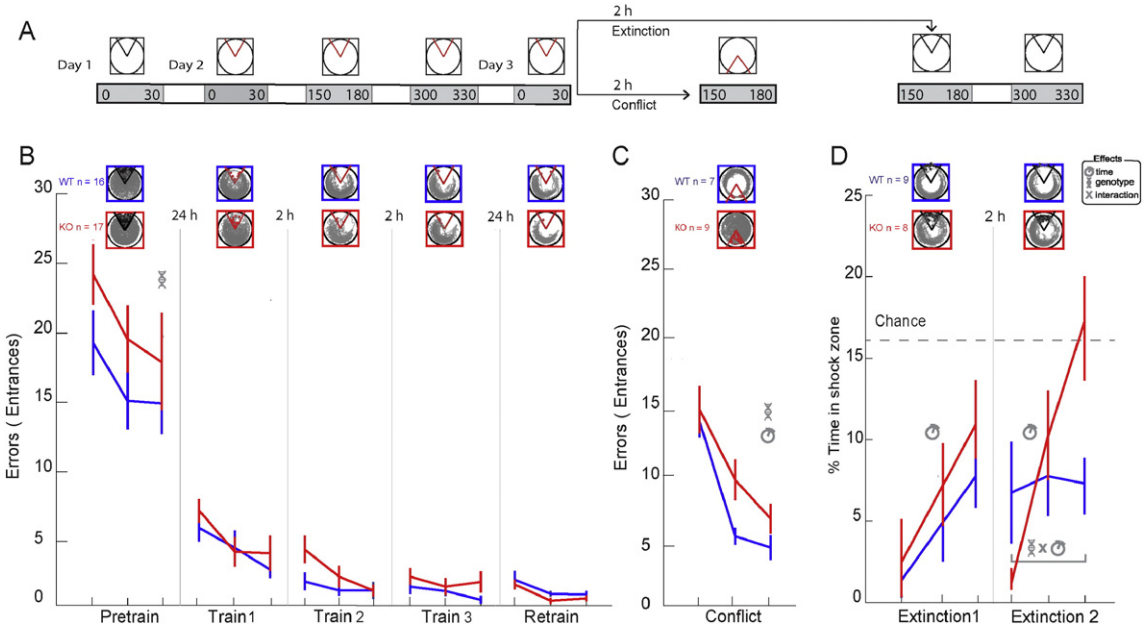

Fig. 2. Cognitive discrimination is selectively impaired in Fmr1 KO mice. (A) The active place avoidance protocol. All sessions were 30 min and separated by 2-h breaks within a day. On Day 1 shock was off during the pretraining session. Three 30-min training sessions with shock on were administered on Day 2 to measure learning. A retraining session was administered on Day 3 to measure 24-h retention of the conditioned avoidance. After a 2-h break, to measure cognitive discrimination, one group of animals received conflict training with the shock zone moved to the opposite location. The other group received two extinction training sessions with the shock turned off. The second extinction session emphasized cognitive discrimination to distinguish between the initial shock on and recent shock off conditions. (B) Place avoidance measured as a reduction in errors (entrances into the shock zone) during the pretraining, training and retraining sessions. Fmr1 KO (n = 17) and WT (n = 16) mice explored the whole arena during pretraining, with gradual habituation. The KO mice were more active. Place avoidance performance was similar when shock was turned on. The errors rapidly reduced within and between sessions across 2-h and 24-h retention intervals. Each tick on the x-axis indicates a 10-min epoch within the 30-min session. Tracks from each session for single representative WT and KO mice are shown. (C) Place avoidance in both the WT (n = 7) and KO mice (n = 9) is initially and similarly disturbed on the conflict session. The WT mice learn to avoid the new shock zone faster than the KO mice. (D) Place avoidance during the first extinction training, measured by time in the initial shock location, was similar between the WT (n = 9) and KO (n = 8) mice. In contrast, the groups differed when the mice were returned to the arena for the second extinction session. Note that the KO mice initially behaved as if avoidance was fully reinstated. However, with continued extinction experience, the KO mice completely extinguished the avoidance, reaching chance performance, whereas the WT mice maintained an intermediate level of avoidance throughout the second extinction session. Legend: significant ANOVA effects indicated by the symbols: helix — genotype, clock — time.

however we did not analyze this band because this electrode site was only sampled in two animals. Each blob in the comodulogram is characterized by three potentially independent features, the frequency of the fast modulated oscillation, the frequency of the slow modulating oscillation, and the strength of the phase–amplitude coupling. Here we focus on the modulation index (MI) that measures the strength of the theta-phase modulation of the gamma amplitude (see Fig. S2 for discussion of the modulated and modulating frequencies). By inspection, theta-phase modulation of gamma appeared greater during pretraining than the training sessions but there were no reliable genotypic differences (Fig. 3A–C). During the two extinction sessions the modulation appeared to decrease in the LFP at *stratum pyramidale* of WT mice whereas it appeared to increase in the Fmr1 KO. We examined and quantified these impressions in 10-min epochs during each 30-min session (Fig. 3C). Because running speed varied within and between sessions (Fig. 3D) and speed modulates both theta and gamma oscillations (McFarland et al., 1975; Chen et al., 2011; Ahmed and Mehta, 2012), we included speed as a covariate in statistical evaluations. We began by comparing peak MI in the WT and KO mice during 10-min epochs of the pretraining session (genotype: $F_{1,16} = 2.70$; $P = 0.12$; time: $F_{2,15} = 3.84$; $P < 0.05$; genotype × time interaction: $F_{2,15} = 0.60$; $P = 0.6$). During the first 10 min of pretraining, PAC at the pyramidal cell layer was greater than it was during the last 10 min ($t_{17} = 2.57$; $P = 0.02$). Accordingly, subsequent analyses also took the time during a session into account.

We investigated the effects of the various task phases and manipulations on theta–gamma PAC at *stratum pyramidale* using genotype × session ANCOVA. The results are summarized in Table 1. To assess the impact of introducing shock we compared the first 10 min of the pretraining session and the first 10 min of the first training session to minimize within-session time effects. The effects of genotype and session were significant because PAC was greater in the Fmr1 KO and it decreased in both genotypes when shock was introduced. While learning across the place avoidance training trials had no detectable effects, the 24-h retention period caused PAC to increase in the Fmr1 KO, which resulted in significant effects of session and the genotype × session interaction. PAC at *stratum pyramidale* did not differ across the conflict and extinction sessions when the genotypes differed in place avoidance (Table 1). Note that in these recordings the environment was identical across all the sessions except during the 500 ms periods when shock was delivered, and that the physical manipulations were the addition, change of location, or removal of the transient shock. These analyses of PAC in the LFP at *stratum pyramidale* suggest that PAC is mostly insensitive to such subtle manipulations. We next explored the alternative, that the modest session-specific variations of PAC at *stratum pyramidale* might be part of a more dramatic pattern of changes in PAC within the somato-dendritic functional-anatomical organization of the hippocampal LFPs.

2.4. Cognition-dependent phase–amplitude coupling in Fmr1 KO mice as abnormal trajectories through a hippocampal oscillatory state space

The effects of the behavioral manipulations on PAC at *stratum pyramidale* were modest, but what about the pattern of PAC across the somato-dendritic axis of dorsal CA1? Whether anatomically-organized neural coordination differed as the cognitive demands changed across the behavioral sessions was evaluated. A neural activity vector comprised of the site-specific values of PAC obtained only from periods of time when mice were moving (speed >3 cm/s) was computed. This estimate is analogous to the use of spike train activity vectors to estimate dynamical representational states of hippocampus (Gothard et al., 1996; Pastalkova et al., 2008; Fenton et al., 2010; Kelemen and Fenton, 2013). We focused on the peak theta–gamma normalized modulation index (MI) at each site, although the activity vectors could have been defined by the additional oscillatory features we analyzed (e.g. Fig. S2). Fig. 4A depicts the genotype-averaged MI activity vectors for each behavioral session. By inspection, both genotypic and session-specific differences are apparent. Theta–gamma PAC at the molecular layer of the dentate gyrus (DGm) and the *stratum pyramidale* sites, the neocortical input and outputs of the trisynaptic loop, appears generally stronger at these sites in the Fmr1 KO than the WT, although the coupling also changes across sessions. Comparing these PAC activity vectors in a cross-correlation matrix highlights multiple features of the across session dynamics (Fig. 4B). Whereas the pattern of PAC values becomes less correlated between the pretraining and first training sessions, this modulation of PAC is attenuated in the mutant, which maintains a high correlation. Similarly, the correlation between the site-specific pattern of the PAC activity vectors during the retention and conflict sessions is reduced in WT mice but much less so in Fmr1 KO mice (white squares highlight these regions of interest).

We then visualized the vectors as points in the space defined by the PAC activity at the selected electrode sites. The WT and KO session-sequence trajectories through this space, and 3-D and 2-D cuts through this space are shown in Fig. 4C and D, respectively. These illustrate that the WT and KO trajectories are largely segregated. Three patterns are apparent. First, in WT mice, the strength of PAC at the DGm and slm neocortical inputs appears relatively correlated across the sites, as if there is a maintained balance in these ECII inputs to hippocampus (Fig. 4D1). A similar balance is observed between the DGm input and the sp output regions (Fig. 4D2). These patterns of relationship are less apparent in the KO. The second pattern is that the coordinated

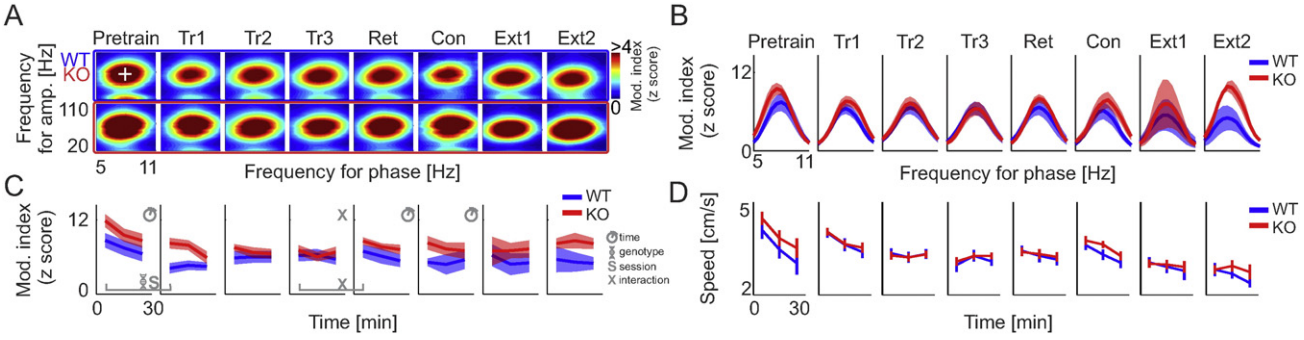

Fig. 3. Theta–gamma phase amplitude coupling at *stratum pyramidale* of wild type and Fmr1 KO mice. (A) Average PAC comodulograms computed for all frequency combinations between the 5–11 Hz theta band and the 20–110 Hz gamma band across experimental sessions (columns). Data from wild type and Fmr1 KO mice are marked by blue and red rectangles respectively. Color corresponds to the normalized modulation index (z score). (B) Vertical (gamma band) comodulogram profile taken at the peak theta frequency of the theta–fast gamma modulation (white cross in A top, left). Blue traces correspond to the wild type mice, red traces to the Fmr1 KO mice. Standard error is shown as a transparent area. (C) Peak fast gamma PAC frequency across electrode locations and experimental sessions. Data were computed in three 10-min epochs for each session. (D) Average animal speed computed from the same 10-min epochs as used in D. Legend: significant ANCOVA effects indicated by the symbols helix — genotype, S — session, clock — 10-min session epoch.

Table 1
Effects of training manipulations on PAC at *stratum pyramidale*: summary of genotype × session ANCOVA results with speed as the covariate. Bold indicates significant effects.

Manipulation	Comparison session.10-min epoch	Genotype	Session	Genotype × session interaction
Introducing shock	Pretraining.1 vs Training 1.1	$F_{1,12} = 9.71$ $P = 0.009$	$F_{1,12} = 7.04$ $P < 0.02$	$F_{1,12} = 0.36$ $P = 0.56$
Learning	Training 1.1 vs Training 3.1	$F_{1,11} = 3.52$ $P = 0.09$	$F_{1,11} = 0.004$ $P = 0.95$	$F_{1,11} = 1.91$ $P = 0.19$
24-h retention	Training 3.1 vs Retention.1	$F_{1,15} = 0.99$ $P = 0.33$	$F_{1,15} = 10.7$ $P = 0.005$	$F_{1,15} = 4.63$ $P < 0.05$
Conflict	Training 3.1 vs Conflict.1	$F_{1,6} = 0.25$ $P = 0.63$	$F_{1,6} = 1.19$ $P = 0.32$	$F_{1,6} = 3.2$ $P = 0.13$
Extinction start	Retention.1 vs Extinction 1.1	$F_{1,7} = 0.18$ $P = 0.68$	$F_{1,7} = 2.56$ $P = 0.15$	$F_{1,7} = 0.91$ $P = 0.37$
Extinction end	Retention.3 vs Extinction 1.3	$F_{1,7} = 1.81$ $P = 0.22$	$F_{1,7} = 0.59$ $P = 0.46$	$F_{1,7} = 0.03$ $P = 0.86$
Retention of extinction	Extinction 1.1 vs Extinction 2.1	$F_{1,7} = 0.16$ $P = 0.70$	$F_{1,7} = 0.008$ $P = 0.93$	$F_{1,7} = 0.29$ $P = 0.30$

neural activity recorded from the WT mice occupies a more constrained region of the vector space with less extreme values of the modulation strength compared to the mutants. This is even seen at the start of pretraining during which the Fmr1 KO mice express relatively exaggerated PAC at DGm and sp (Fig. 4D2). This observation was quantified by computing the average Euclidean distances between the session-specific PAC activity vectors and the session- and genotype-averaged vectors (Fig. 4E upper). The genotype × session 2-way ANOVA confirmed a main effect of genotype $F_{1,102} = 8.47$; $P = 0.005$ but not effects of session and the interaction. We also computed the average Euclidean distances between the session-specific PAC activity vectors and the genotype-averaged vectors for each session (Fig. 4E lower). Similarly, the mutant distances were generally greater than the WT distances and only the effect of genotype was significant ($F_{1,102} = 35.9$; $P = 0.007$). The third observation is focused on the conflict and extinction sessions in which the concurrent place avoidance behavior of the Fmr1 KO mice is abnormal. The conflict and extinction sessions cause the activity vector trajectories of both genotypes of mice to move in somewhat different directions, reducing modulation at all the sites during the conflict session relative to the extinction sessions in both genotypes. Whereas the WT activity vector during the conflict session shifts away from the region that is occupied by the training vectors, the vector in the mutant tends to occupy the same region as the training vectors, despite the shock zone being different. It is as if this WT pattern of coordinated neural activity has changed between the initial training and conflict conditions along with the experience of the location of

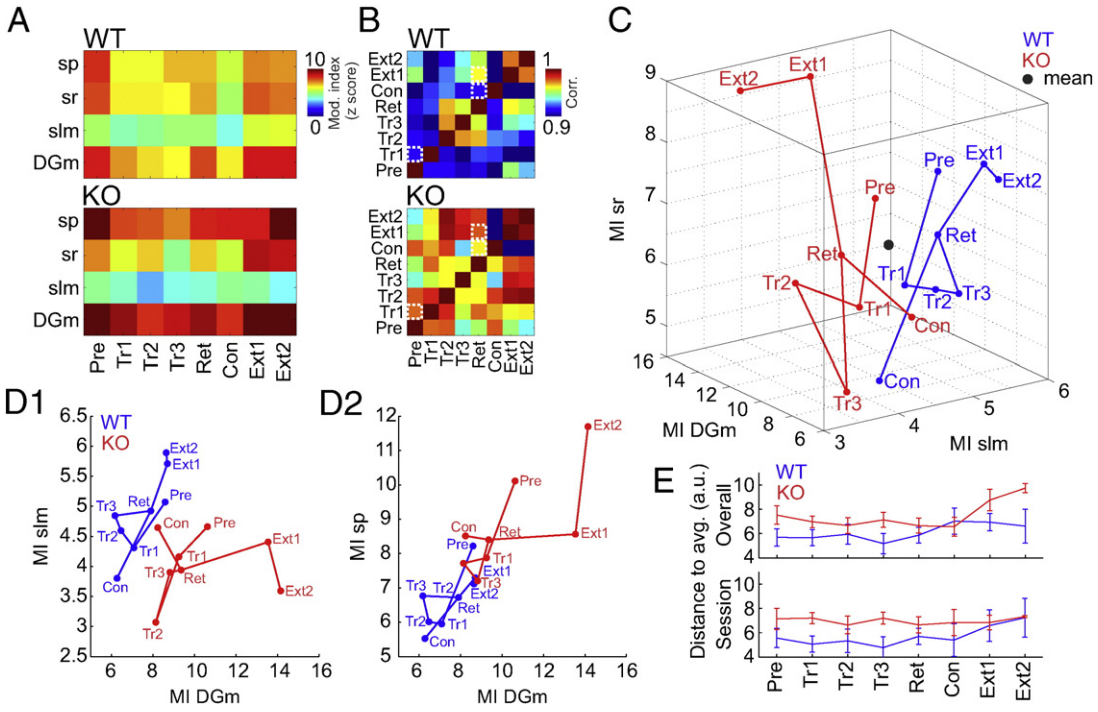

Fig. 4. The somato-dendritic pattern of theta–gamma phase amplitude coupling changes across the behavioral protocol illustrating that discoordination in Fmr1 KO mice depends on cognitive challenge. (A) The group-averaged normalized peak modulation index (z score) for each behavioral session is depicted as a vector across the 4 indicated electrode locations and experimental sessions. (B) Cross-correlations between all pairs of the session-averaged 4-D vectors. Overall, the correlations tend to be lower (cooler colors) in WT than in the Fmr1 KO (hotter colors) mice, indicating differences in across-session variability of the oscillatory activity patterns. The dotted white squares highlight when the mice encountered changes in the shock zone; trial 1 (addition of shock), conflict (change of shock) as well the first extinction session (the absence of shock). (C, D) The PAC activity vector drawn as a trajectory through C) the 3-D subspace defined by PAC on the input regions and D) two 2-D subspaces defined by the input and output regions of the CA1 circuit. The genotypes occupy largely non-overlapping portions of these subspaces and the session-specific vectors move within the space. WT and KO PAC tends to be balanced between the sites that define the 2-D subspaces (i.e. PAC values fall along diagonal axes), but in extinction sessions there is a disbalance in the KO (PAC values deviate from the diagonals). The session abbreviation is indicated at the corresponding points in the subspaces. E) Quantification of the deviation of the session-specific vectors from the centroid of all the activity vectors (indicated by a black dot in panel C). The deviation is measured as the Euclidean distance in the 4-D space.

shock, but this change was less apparent in the mutant mice. The genotypic differences are even more distinct on the extinction sessions. The MI values in the WT increase modestly during the extinction sessions and move to the vicinity of the pretraining vector, when shock was also off. In contrast, the MI values in the KO increase strongly at most recording sites, especially the sr and DGm sites, such that the activity pattern moves far from the region of that is occupied by the pretraining vector. It is as if the WT pattern of coordinated neural activity reverted to the pretraining pattern, consistent with shock being absent in the two session types, but the corresponding neural activity in the mutant changed to some extreme pattern that had not been previously expressed.

In summary, a dynamical view of the electrophysiological state of theta–gamma PAC illustrates that the overall somato-dendritic patterns and changes of the Fmr1 KO and WT hippocampal activity patterns are distinctive in that the relative amounts of PAC at the specific sites tend to differ between the training and conflict conditions in the WT but tend to be more preserved in the Fmr1 KO. Whereas, on the extinction sessions there is an extreme response in the Fmr1 KO compared to the WT. We conclude that the spatially and temporally coordinated patterns of neural coordination between theta and gamma oscillations are modulated by cognitive effort and/or information processing and that this coordination is abnormal in the Fmr1 KO mouse.

2.5. Cognition-dependent oscillatory phase-synchrony abnormalities in Fmr1 KO mice

We then evaluated the assumption that neural coordination is necessary because different types of information arrive at the different CA1 inputs. We analyzed band specific phase synchrony between pairs of LFP from the sp, sr, and slm sites. The conjecture that slow and fast gamma oscillations are associated with different information streams predicts that gamma phase synchrony will be modulated by genotype, oscillation frequency, and behavioral session in a pattern that is specific to the electrode pair (Colgin et al., 2009; Fries, 2009). There were three specific predictions: 1) sp–sr and sp–slm gamma phase-synchrony will be greater than sr–slm synchrony, because sr and slm inputs carry distinct information; 2) In the conflict session, WT mice will reduce sp–sr synchrony because the influence of sr on sp activity is reduced to bias CA1 output in favor of slm activity (i.e. data/encoding will dominate memory/recall); 3) WT and KO gamma-phase synchrony will differ during the second extinction session with sp–sr synchrony greater in the KO than WT because KO mice are more strongly influenced by the initial shock zone location (i.e. memory/recall will dominate data/encoding).

Fig. 5 shows frequency band-specific phase synchrony, computed using debiased weighted phase lag index (dWPLI) between the sp–sr, sp–slm and sr–slm pairs of sites. Phase synchrony is modulated by speed. For example, collapsing the data across genotype and the pairs of electrode sites, the speed X dWPLI correlations were significant for the theta ($r = -0.2$; $P = 10^{-3}$) and beta bands ($r = -0.2$; $P = 10^{-3}$) and for specific sessions and electrode pairs, the speed X dWPLI correlation was also significant in the slow and fast gamma bands. Consequently we included speed as a covariate in subsequent statistical evaluations. Although phase synchrony was typically greater for slower frequency bands (i.e. theta > beta > slow gamma > fast gamma) the speed covariate was sufficient to account for all apparent frequency band effects because no frequency effects were significant once dWPLI was corrected for speed.

The two-way genotype × frequency band ANCOVAs performed on the sp–sr phase synchrony data revealed significant effects of genotype in both the first ($F_{1,24} = 9.54$; $P = 0.005$) and second extinction sessions ($F_{1,24} = 17.1$; $P = 10^{-4}$). This was due to increased synchrony in the KO (Fig. 5A). The pattern of phase synchrony between the sp and slm sites was different (Fig. 5B); the genotype effect was only significant during the first training session when WT synchrony was greater ($F_{1,48} = 6.44$; $P = 0.01$) and the second extinction session when KO synchrony was greater ($F_{1,16} = 6.83$; $P = 0.02$). The pattern of phase synchrony between sr and slm showed significant genotype effects only on the conflict ($F_{1,44} = 5.92$; $P = 0.02$), extinction 1 ($F_{1,44} = 5.31$; $P = 0.03$) and extinction 2 sessions ($F_{1,44} = 6.63$; $P = 0.01$) that test cognitive discrimination (Fig. 5C). Thus phase synchrony tended to differ between the genotypes especially when processing novelty and cognitive discrimination was required.

These phase synchrony measures were next compared between pairs of sessions using two-way genotype × session ANCOVAs, with speed as the covariate. To investigate the effect of introducing shock at the start of place avoidance training, we compared synchrony between the pretraining and first training session with shock. Introducing shock did not influence phase synchrony between sp and sr However, between sp and slm the effect of session was significant at theta frequencies ($F_{1,12} = 6.54$; $P = 0.03$) with a marginally greater decrease in the KO mice (interaction: $F_{1,12} = 4.73$; $P = 0.05$). The effect of genotype was significant at beta frequencies ($F_{1,12} = 4.74$; $P = 0.05$) due to a decrease in KO mice. Theta coupling was decreased between sr and slm in the KO, while synchrony was unchanged in the WT as demonstrated by a significant genotype × session interaction at theta frequencies ($F_{1,24} = 4.93$; $P = 0.04$).

Next, to investigate the effect of learning across place avoidance training, we compared synchrony between the first and third training sessions with shock. The effect of genotype on slow gamma synchrony between the sp and sr sites was significant due to higher synchrony in the KO ($F_{1,15} = 4.74$; $P < 0.05$). In contrast, theta synchrony between sp and slm was higher in the WT ($F_{1,12} = 9.04$; $P = 0.01$).

To examine the effect of the 24-h retention period we compared phase synchrony during the third training and the retraining sessions. No genotypic or session differences were observed at any pair of electrodes (F's < 3.3; P's > 0.09), mirroring similar retention of the avoidance in Fmr1 KO and WT mice.

We were especially interested in whether synchrony changes across the conflict session since this is when the KO cognitive deficit is explicit. There was a significant effect of genotype ($F_{1,7} = 11.9$; $P = 0.01$) because beta synchrony in the KO was lower between sp and sr during the conflict session. A similar pattern was observed for beta synchrony between sr and slm ($F_{1,11} = 8.7$; $P = 0.01$). There was also a significant effect of session on slow gamma synchrony between sr and slm due to increased slow gamma synchrony on the conflict session ($F_{1,11} = 4.93$; $P < 0.05$).

We were also interested to investigate changes in synchrony in the WT and Fmr1 KO mice when shock was turned off to evaluate extinction of the place avoidance. There was an effect of genotype on fast gamma synchrony between sp and slm due to higher synchrony in the KO ($F_{1,4} = 7.92$; $P < 0.05$). Comparing phase synchrony across the 24-h retention and second extinction sessions showed a significant effect of genotype on fast gamma synchrony between sp and slm because the WT mice reduce synchrony during extinction learning ($F_{1,4} = 7.93$; $P < 0.05$). Theta synchrony between sr and slm was reduced in the WT, causing a significant genotype effect ($F_{1,11} = 5.18.$; $P = 0.04$). Investigating the changes in synchrony across the two extinction sessions showed a single significant effect of genotype on theta synchrony between sr and slm ($F_{1,11} = 6.21$; $P = 0.03$) due to greater dWPLI in the KO.

While these frequency-, electrode location-, and genotype-specific differences in phase synchrony are likely influenced by volume conduction (Buzsaki et al., 2012), this influence was minimized by computing dWPLI as the measure of phase synchrony (Vinck et al., 2011). Furthermore, the constellation of differences, especially those that appear only during the cognitive discrimination challenges of the conflict and extinction sessions, argue strongly that they arise from different cognition-dependent sources. In particular, gamma phase synchrony tended to decrease between the two CA1 inputs (sr and slm) as well as between these inputs and the CA1 output (sp) in response to the

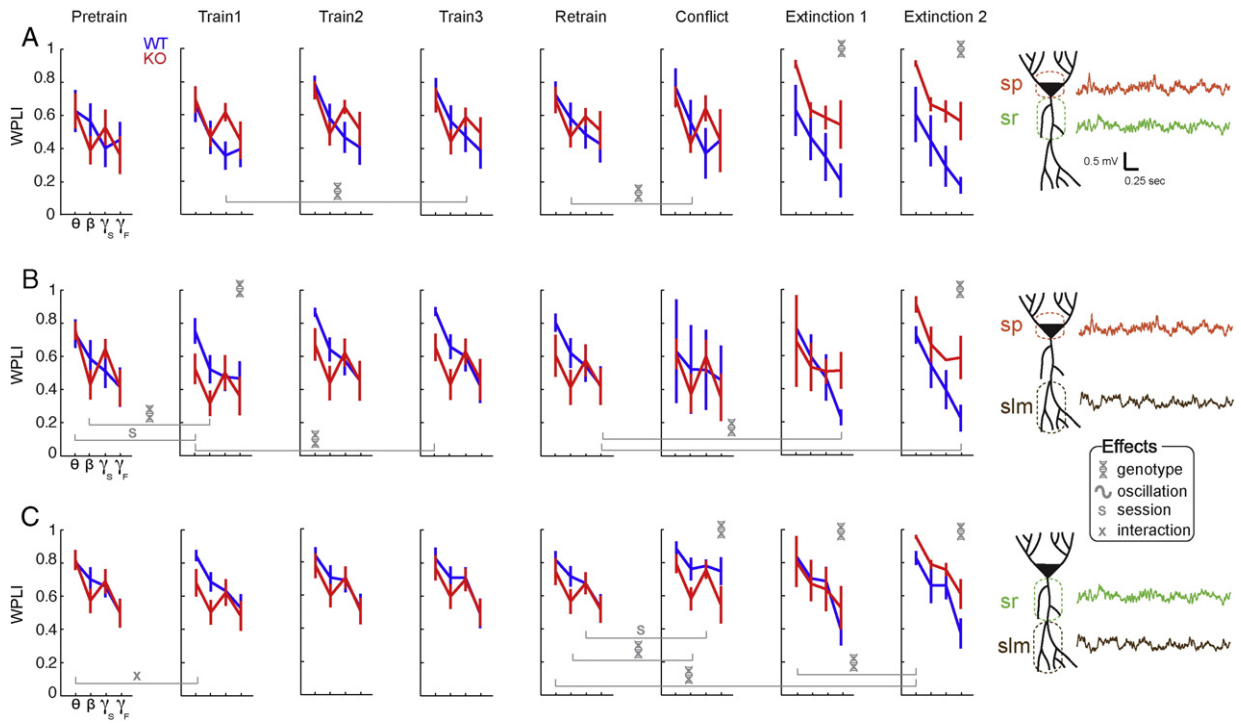

Fig. 5. Intrahippocampal frequency-specific phase synchrony is altered in Fmr1 KO mice depending on the cognitive demand. (A) Phase synchrony between the sp and sr sites was typically strong, with dWPLI ~0.5 at all frequencies during pretraining and the initial training sessions. Phase synchrony in extinction sessions is higher in KO than in WT across all bands. B) Phase synchrony between the sp and slm sites in the theta and beta bands is higher in WT than in KO during training and retraining sessions. During the extinction sessions WT mice tended to decrease coupling, especially at faster frequencies, whereas the decrease was absent in KO mice. (C) Phase synchrony between the sr and slm sites is higher in the theta and beta bands of WT compared to Fmr1 KO mice during the first training and conflict sessions. During the second extinction session, phase synchrony was decreased, especially at faster frequencies, and was lower in WT than KO across all bands. Legend: significant ANCOVA effects indicated by helix — genotype, tilde — oscillation, S — session, and X — interactions. ⌴ — indicates significant oscillation band-specific comparisons between the indicated pairs of sessions. The example raw LFP traces are from a WT mouse.

demand for cognitive discrimination. These decreases tended to be greater in the WT than the Fmr1 KO mice, suggesting differential information processing. Together these observations are consistent with the predictions from the discoordination hypothesis that sp–sr and sp–slm oscillatory synchronies are distinct and that the patterns between the two genotypes change in the conflict and extinction sessions when the KO mice demonstrate cognitive impairments.

3. Discussion

3.1. Summary

We find that spatial learning (Fig. 2) and the power of oscillations in hippocampal LFPs appear essentially normal in Fmr1 KO and WT mice (Fig. S1) but that the KO mice express deficits in cognitive discrimination, abnormal coordination of site-specific hippocampal theta and gamma oscillations (Figs. 3, 4), and abnormal input-specific oscillation phase synchrony (Fig. 5), especially when they are challenged to discriminate between conflicting memories. This pattern of spared and impaired behavior and neural activity is predicted by the discoordination hypothesis that aberrant neural coordination underlies deficits in the judicious use of information (see review, Fenton, 2015). Although, the somato-dendritic pattern of theta–gamma PAC is generally abnormal in Fmr1 KO mice, the conjoint Fmr1 KO deficits in cognitive discrimination and neural coordination were specifically observed when the shock zone was in an unfamiliar location on the conflict trial as well as when it was turned off on extinction trials. Exaggerated extinction learning in Fmr1 KO mice has been reported for inhibitory avoidance (Dolen et al., 2007) and an instrumental visual discrimination task (Sidorov et al., 2014). We observed a more complex, dynamic pattern of abnormality. Extinction in the KO was normal when shock was first turned off, but it was under and then over expressed at the start and at the end of the second extinction session, respectively (Fig. 2D). The deficit we observed in the conflict and extinction tasks is different from the deficit that is expressed by mice with reduced adult neurogenesis in the dentate gyrus (Burghardt et al., 2012; Park et al., 2015). Mice with ablated neurogenesis express normal extinction, and they persist in avoiding the initial shock zone on conflict trials more than controls, whereas on conflict trials Fmr1 KO mice did not perseverate more than controls, yet their conflict learning was impaired. These data provide evidence that initially learning and retaining information is normal in Fmr1 KO mice but loss of FMRP causes a deficit in the ability to judiciously use information that conflicts with what had been initially learned.

The Fmr1 KO deficit in cognitive discrimination is accompanied by an abnormal functional–anatomical pattern of temporally coordinated neural activity. On the conflict trial, WT mice minimized theta–gamma PAC at each input (mDG, slm, sr) and the output (sp) that we assessed, consistent the notion that the prior pattern of neural activation is suppressed along with the initially conditioned place avoidance behavior. In contrast to WT mice, Fmr1 KO mice modified the oscillatory pattern of activity at the inputs and outputs much less, suggesting they did not sufficiently modify their neural activity representation of the environment, which was maladaptive, compared to WT mice. This is not to say that loss of FMRP leads to a general blunting of neural responses to representational demands because a different pattern of findings was observed when shock was turned off for the extinction trials. Here the WT pattern of oscillations changes less than it did in the Fmr1 KO mice. In fact, the KO mice expressed an unusual and extreme pattern of neural activity on the extinction trials (Fig. 4). This suggests the KO mice overreacted and may have tried to represent the environment differently, whereas the WT mice did not express an unusual pattern of theta–gamma PAC, and as such probably did not change the representation of the environment. These observations extend behavioral

observations of exaggerated responses to environmental change in Fmr1 KO mice (Moon et al., 2006; Moon et al., 2008) by demonstrating an exaggerated adjustment of representational neural activity in the KO mice upon experiencing changes in the location of shock (Figs. 3, 4 and 5). Based on the present recordings we speculate that KO mice may have treated the environment as radically different, in contrast to WT mice that probably recognized the environment was the same and that only the shock location changed. While the present observations are consistent with the notion of excessive neural processing in subjects with autistic features (Markram et al., 2007), they do not explain the reinstatement of avoidance in the KO mice at the start of the second extinction session, which suggests almost the opposite, a failure to distinguish between the memory for the initial shock zone and the memory for no shock in the most recent session. These findings predict that in response to environmental changes Fmr1 KO mice have both exaggerated and blunted updating of their neural representations of the environment that amount to maladaptive behavior in both instances. We note that the pattern of genotypic differences in neural coordination appears to reflect differences in response to novelty and cognitive discrimination, in addition to the baseline alterations due to loss of FMRP. These genotypic differences in neural activity, especially those that did not coincide with cognitive deficits, may, at least in part, also reflect compensatory changes in information processing due to baseline differences in synaptic function that may result from loss of FMRP (Comery et al., 1997; Braun and Segal, 2000; Bassell and Warren, 2008).

3.2. Spatial and temporal coordination of neural activity

The magnitudes and patterns of LFPs vary strongly across somatic and dendritic locations within the hippocampus (Bragin et al., 1995; Csicsvari et al., 2003b) and these signals vary with behavior and cognition (Montgomery and Buzsaki, 2007; Tort et al., 2008; Montgomery et al., 2009). We also find electrode site-specific and task-specific variations in hippocampal LFPs, which were especially pronounced in the theta phase modulation of gamma oscillations (Figs. 3, 4). Despite volume conduction between the electrode sites, which may contribute to the relatively high similarity of power spectra across electrode sites (Fig. S1), the recordings were sufficiently local because features like theta phase and amplitude as well as estimates of neural coordination were quite distinct between electrode sites (Figs. 1B and C, 3 and 5). The LFPs at the DGi electrode were qualitatively different between the KO and WT mice because this was the only site at which theta-modulated slow gamma was observed as distinct from fast gamma, but only in KO mice (Fig. S3). It would be valuable in future work to investigate if this is related to the alteration of synaptic potentiation and depression in the perforant path input to DG that has been reported in Fmr1 KO mice (Eadie et al., 2012), and the persistent changes in responses to perforant path stimulation that are caused by place avoidance training (Park et al., 2015). Alternatively, the origin of the slow gamma may be the appearance of events such as dentate spikes with a similar frequency footprint as slow gamma oscillations (Kramer et al., 2008). Alternatively, the origin of the slow gamma may be nearby CA3, which should motivate future studies to record from sites across the coronal plane too.

The most significant differences in theta–fast gamma PAC between the Fmr1 KO and WT mice tended to be at the CA1 sp, a site of strong perisomatic inhibition and the DGm, a major site of the perforant path input. These differences in neural coordination along with the phase synchrony between sites, strongly depended on session indicating the electrophysiological differences reflect internal, cognitive variables because the sessions were physically identical whenever shock was not on, which was typically 97.5% of the time at the start of the conflict session and was typically more than 99% in other sessions with shock.

Prior work suggested that fast gamma oscillations recorded at sp in rat carried information about current experience ("data encoding") thought to be from the entorhinal cortex which synapses at CA1 slm, and that slow gamma carried information from CA3, representing memory and expectations ("model retrieval"), which synapses at CA1 sr (Colgin et al., 2009; Fries, 2009; Bieri et al., 2014). Although we can detect theta–slow gamma PAC at sp of the rat hippocampus (Dvorak and Fenton, 2014) these signals were not seen as distinct from fast gamma in the mouse (Fig. 3, S2), despite substantial gamma oscillation power (Fig. S1). According to the data/encoding-model/retrieval concept, one might have expected to see a relative increase in slow gamma over fast gamma on the memory retention session and a relative decrease in the ratio on the conflict and extinction trials when memory for the initial shock zone should be suppressed, but this was not observed. The data/encoding-model/retrieval concept can appear to suggest that fast gamma will be local to slm and slow gamma local to sr, in accord with the local entorhinal and CA3 inputs to CA1, respectively. However, we see no evidence of this (Figs. S2, 5) and it is more likely that these inputs tonically drive inhibition that manifests as gamma oscillations at perisomatic sites (Kiss et al., 1996; Penttonen et al., 1998; Papp et al., 2001; Klausberger et al., 2003; Lasztoczi and Klausberger, 2014) due to feedforward GABAA receptor activation (Traub et al., 1996; Wang and Buzsaki, 1996). Accordingly, the coordination of fast and slow gamma oscillations in CA1 reflects coordination of potentially conflicting information arriving at sr and slm. It is thus remarkable that we mainly observed modulation of theta-coupled fast gamma oscillations, as if slow gamma oscillations were more or less continuous and not phase locked to theta (Schomburg et al., 2014). In addition, as seen in Fig. S2C, on the conflict session the frequency of the theta-modulated fast gamma oscillations in WT mice increased at the slm and DGm sites of the entorhinal input, and they tended to decrease on the extinction sessions, suggesting elevated and suppressed entorhinal input on the conflict and extinction sessions, respectively. This pattern of coordinated changes was not observed in the KO mice, providing additional evidence of aberrant coordination of cognition-related neural oscillations, as predicted by the discoordination hypothesis.

3.3. Targeting neural coordination: neural discoordination as the FXS pathophysiology

The present findings confirm predictions of the discoordination hypothesis that aberrant neural coordination underlies cognitive dysfunction after loss of FMRP. This hypothesis emerges from a systems approach to understanding cognition and conceptualizing FXS, which has not been the norm in FXS research. Naturally, research has focused on the molecular and biochemical changes that result from loss of FMRP and potential compensatory and therapeutic targets (Tamanini et al., 1996; Hagerman et al., 2010; Sharma et al., 2010; Bhattacharya et al., 2012). This is partly because of the impressive progress in understanding FXS, which began by identifying the cause (Pieretti et al., 1991), a CGG trinucleotide repeat expansion exceeding 200 repeats, leading to loss of FMRP and then modeling it by deletion of Fmr1 in mice (Bakker et al., 1994) and recently rats (Till et al., 2015). In vitro physiological investigation was then successful in characterizing and delineating synaptic dysfunctions that are associated with Fmr1 KO. This established dysregulation of mGluR-stimulated translation and synaptic plasticity as the dominant hypothesis (Bear et al., 2004) and it has provided a tenable therapeutic target (Erickson et al., 2013). Unfortunately there have been difficulties with efficacy according to FDA standards in Phase 3 clinical trials (Berry-Kravis et al., 2012), as reported in the press (Pollack, 2013). It seems that, even with such a well-defined etiology, FXS may have diverse symptomatology, as the proximal causes of the disorder interact with developmental and environmental influences, and this seems to be the norm for many forms of mental dysfunction (Smoller JWC-DGotPGC, 2013).

It is important to acknowledge that loss of FMRP did not detectably impair standard place avoidance learning or memory and neither were LFPs substantially abnormal during the initial task presentation

despite this place avoidance variant being an especially sensitive assay of hippocampal integrity (Cimadevilla et al., 2001; Kubik and Fenton, 2005; Wesierska et al., 2005; Pastalkova et al., 2006) and a cause of functional plasticity (Park et al., 2015). This demonstrates, like others have reported, that following loss of FMRP, basic learning and memory dysfunction is not reliably associated with the absence of FMRP, despite clear and robust abnormalities in molecular and cellular synaptic function, (Godfraind et al., 1996; D'Hooge et al., 1997; Bakker and Oostra, 2003; Vanderklish and Edelman, 2005; Auerbach and Bear, 2010; Krueger et al., 2011; Bhakar et al., 2012; Eadie et al., 2012; Osterweil et al., 2013), including plastic in vitro responses to stimulus trains derived from place cell spike trains (Deng et al., 2011). In contrast, the present work identified robust alterations in LFP coordination as well as altered associations between cognitive and LFP coordination abnormality during cognitive discrimination challenges. Theta–gamma PAC was higher or lower in the KO or WT depending on where it was recorded, on what behavioral trial it was recorded, and even if the mouse was moving fast or slow. This is strong evidence that the presence, exact nature, and relevance to cognitive function of the neural function abnormalities we detected could not have been identified in baseline, or even single training trials. In order to characterize the abnormality, which was not simply too little or too much PAC, it was necessary to assay neural function at multiple sites and across different cognitive behavioral states. This highlights the importance of studies that evaluate multiple levels of neural system function in individual subjects. Because there is great diversity in the molecular consequences and symptoms, even when disease etiology is specific like silencing of FMR1, we have adopted a neural systems approach and hypothesize there may be a common pathophysiology at the level of neural coordination to account for cognitive discrimination impairments (Mitchell et al., 2013; Fenton, 2015).

Here we identified in Fmr1 KO mice cognition-associated neural discoordination at the level of theta–gamma phase amplitude coupling and phase synchrony between perisomatic and dendritic sites of hippocampus. It is our contention that such abnormalities manifest in diverse cognitive networks of subjects lacking FMRP because neural coordination in general, and cross-frequency coupling in particular, is a form of neural computation central to complex cognition because it is necessary to synchronize information processing between distant as well as within local neural circuits (Lakatos et al., 2005; Canolty et al., 2006; Buzsaki, 2010; Lisman and Jensen, 2013; Dvorak and Fenton, 2014; Schomburg et al., 2014). Cross-frequency coupling of neural oscillations can be recorded at scalp electrodes during cognitive tasks making them accessible for clinical investigation (Sauseng et al., 2009). As shown here, standard measures of oscillatory power were not abnormal whereas cross-frequency coupling was discoordinated under cognitive challenge. The hope is that the use of cross-frequency coupling can allow differentiation of FXS patients into subclasses on the basis of identified pathophysiology that is driving symptoms. Not only might this allow better matching of patients and treatments for clinical trials and clinical management, but the brain stimulation technologies and behavioral therapies that are in development such as TMS, DCS, and DBS, may themselves one day target neural coordination phenomena to correct and enhance the neural functions that subserve cognition.

4. Experimental procedures

All methods complied with the Public Health Service Policy on Humane Care and Use of Laboratory Animals and were approved by the New York University and State University of New York, Downstate Medical Center Institutional Animal Care and Use Committees.

4.1. Subjects

Fmr1 null mice (KO) mice carrying the Fmr1^{tm1Cgr} allele were obtained from Jackson Laboratories (Bar Harbor, ME) to establish local colonies. These mice have a mixed C57BL6/FVB background. The background wild-type (WT) mice were used as controls. In total 18 Fmr1 KO and 21 WT mice aged three to six months were used. Data of sufficient quality were obtained and analyzed from 16 WT and 17 KO mice.

4.2. Surgery to implant electrodes

Mice were deeply anesthetized by Nembutal (60 mg/kg i.p.) and mounted in a Kopf stereotaxic frame to implant three bone screws, a reference electrode and a bundle of six recording electrodes. The screw in the frontal bone served as ground and a wire aimed at the cerebellar white matter served as reference. The electrodes were 75 μm Formvar-insulated NiCh wire (California Fine Wire, Grover Beach, CA). The recording bundle was constructed such that the lengths of the individual wires were staggered by 170 μm steps. The tip of the bundle was implanted at −1.80 AP, ±1.30 ML, −1.65 DV relative to bregma, which allowed the electrodes to span ~1 mm in the dorso-ventral axis of the dorsal hippocampus. The electrodes were attached to a Millmax connector that was anchored to the skull and bone screws with one of two dental cements (Grip Cement, Dentsply, Milford DE and TEETs Denture Material, Co-oral-ite Dental Mfg, Diamond Springs, CA). The mice were allowed at least 1 week to recover before experiments began.

4.3. Electrophysiological recording

For electrophysiological recordings, the Millmax electrode connector on the mouse's head was connected to a unity-gain buffering preamplifier that was tethered to the recording system with a lightweight counter-balanced cable. The signal from each channel was referenced to the cerebellar electrode, low-pass filtered (600 Hz) and digitized at 2 kHz using dacqUSB (Axona, St. Albans, U.K.). Initial recordings were made while the mouse was in the home cage and on the rotating arena to screen the electrodes for signal quality. Throughout the study we used narrow-band Finite Input Response (FIR) filters in a zero phase-shift filtering algorithm that were designed using the Matlab Filter Design Toolbox (Dvorak and Fenton, 2014).

In order to map recording sites from individual animals to known anatomical structures we used theta phase and amplitude profiles across sites (Fig. 1B). Instantaneous phase and amplitude information was extracted by band-pass filtering in the theta band (6–10 Hz) followed by the Hilbert transform. Phase and amplitude profiles were then extracted and time-locked at the peaks of the 10% strongest theta oscillations. Theta phase and amplitude profiles were examined to identify which electrode had a fully reversed phase relative to the most dorsal recording site, and which had the largest theta amplitude. Typically the largest theta amplitude was observed at DGm, one electrode below the most dorsal electrode with a full 180° phase reversal. Recordings were only studied if these electrophysiological landmarks were prominent. Across mice, all qualified recordings were put into register with these two landmarks. Histological study confirmed (e.g. Fig. 1B) that the full reversal occurred in the vicinity of the CA1 slm and that the maximum amplitude was observed just below the hippocampal fissure in the molecular layer of the dentate gyrus (DGm) (Buzsaki et al., 2003).

4.4. Histology

When recordings were complete the mice were euthanized by Nembutal overdose (120 mg/kg i.p.) and the brains were prepared for histological assessment of electrode placement. A 10 μA cathodal current referenced to the body was passed for 6–8 s through three of the recording electrodes. These were the most dorsal and ventral electrodes as well as the electrode that was estimated to be at the theta reversal site. Afterwards, the animals were transcardially perfused with 0.9% saline followed by 10% formalin. The brain was removed and

stored in 10% formalin overnight and then cryoprotected in 30% sucrose solution. Transverse 50-μm sections were cut, mounted on gelatin coated glass slides and stained with cresyl violet and 4% potassium ferrocyanide for the Prussian blue reaction (Fig. 1B). The sections were studied by light microscope to identify the electrode locations.

4.5. Active place avoidance

The basic active place avoidance task has been described in detail for mice (Moreno et al., 2011; Burghardt et al., 2012; Kheirbek et al., 2013). Briefly, we modified the commercial system (Bio-Signal Group Corp., Brooklyn, NY) for electrophysiology. The mice were confined to the central region of an 81-cm diameter stainless steel disk by a 40-cm diameter, 50-cm high transparent cylinder made from PETG plastic. The floor was fine copper mesh on which the mice could obtain purchase as they moved. An isolated 500-ms, 60-Hz 0.2–0.3 mA constant current could be delivered across the high impedance of the mouse's paws on the mesh and a low-impedance subcutaneous shock electrode at the neck. Windows-based software (Tracker, Bio-Signal Group Corp., Brooklyn, NY) determined the mouse's location every 33 ms from an overhead video camera by tracking the location of an infrared LED on the preamplifier that was connected to the mouse's head. The software defined a 60° shock zone that was at a fixed location in the room. During training sessions, shock was turned on whenever the mouse entered and remained in the shock zone for 0.5 s. Shock was repeated every 1.5 s until the mouse left the shock zone. Delivery of shock and rotation of the arena at 1 rpm was remotely controlled by the software. The position time series was synchronized to the electrophysiology data time series by video frame TTL pulses.

4.6. Experimental design

We have used the active place avoidance paradigm to investigate cognitive information processing (Fenton et al., 1998; Zinyuk et al., 2000; Kelemen and Fenton, 2010; Kelemen and Fenton, 2013). Place information in hippocampal electrical activity toggles between the distinct stationary and rotating spatial frames during active place avoidance, indicating neural coordination (Kelemen and Fenton, 2010; Kelemen and Fenton, 2013). Theta and gamma oscillations in the hippocampal LFP are primarily expressed during active movement (Vanderwolf, 1969), making contextual fear discrimination, trace fear conditioning and other cognitive discrimination tasks inappropriate if they rely on freezing or do not promote active exploration.

We designed a 3-phase protocol that was optimized for collecting sufficient electrophysiological data during systematically varied cognitive demands. All sessions lasted 30 min. The mouse on the rotating arena was allowed to explore during a pretraining session. After a 24-h rest in the home cage, the mouse was returned to the identical rotating arena for the initial training phase. The only difference is that now the mouse received foot shock whenever it entered the shock zone. Two more training sessions were given, each after a 2-h rest. Retention of the conditioned avoidance was tested after a 24-h rest by a retraining session in conditions that were identical to the training sessions with shock on. The third phase began 2 h later to evaluate cognitive discrimination. We used two task variants. In the conflict task variant, the mouse was returned to the arena with conditions identical to the training phase, except the shock zone was on the opposite side. Because the shock zone is unmarked, the physical conditions of the conflict session are identical to the initial training sessions, except when the mouse is shocked, which for example, is only for 10 s if a mouse receives 20 shocks during a 30-min session. The mice are challenged to distinguish between the two test phases on the basis of that small but important difference (Abdel Baki et al., 2009; Burghardt et al., 2012). An extinction task variant was used to evaluate cognitive discrimination in a second way. When the mice were returned to the arena for the third phase, the conditions were identical to initial training except that shock was turned off. Two extinction sessions were given, each after a 2-h rest. The second session was specifically designed as a cognitive discrimination challenge because it required the mice to discriminate between their memory for when the shock zone was active and the current condition when there was no shock.

4.7. Data analysis

4.7.1. Place avoidance

Place avoidance was evaluated by a number of end-point measures output by TrackAnalysis software. The main estimate of place avoidance was the reduction of errors measured as entrances into the shock zone. On the extinction sessions, the shock was off and avoidance was assessed as the percent time in the location of the former shock zone. This corresponds to 1/6 of the space making chance performance 17%. The mouse's speed was computed every 2 s and the average speed was used to estimate movement during a session.

4.7.2. Preprocessing for LFP recording quality

The LFP data were first processed by a custom artifact rejection algorithm, which identified continuous segments of artifact-free signals. Such segments that were 4 s or longer were used for further analysis. The majority of artifacts were related to the foot shock, specifically signal saturations and slowly changing DC signals as the recording system recovered from the shock artifact. The algorithm was tuned to identify these two types of artifacts. Constant signals close to the maximal voltage of the ADC defined signal saturation. Brief saturations <2.5 ms were allowed. Periods of very low signal variance defined the slowly changing DC signal artifacts. The variance was estimated in a sliding 50-ms long window. Signal epochs with a variance that remained under a predefined threshold for longer than 100 ms were marked as artifacts. The variance threshold was constant through the entire dataset and was selected by visual inspection. Each artifact segment was extended by 1 s on both sides and all artifact-free segments smaller than the 4-s minimum window were also discarded. Each channel in the dataset was processed independently and the algorithm performance was verified by close visual inspection.

4.7.3. Power spectra

Spectral analysis of LFPs was performed using Wavelets because of its ability to extract instantaneous power estimates. First, each LFP signal from the electrode with the highest power in the theta (5-12 Hz) range was selected and z-score normalized in order to remove any amplitude differences caused by electrode impedance variations. Second, the signal was convolved with a group of complex Morlet wavelets in the logarithmic range between 2 and 150 Hz. Third, each time series was squared in order to obtain instantaneous power values for a given frequency. Third, only artifact-free segments when the animal was running (speed above 3 cm/s) were selected and averaged into the resulting spectral estimate. Inter-subject power values were computed separately for the delta (1–3 Hz), theta (5–12 Hz), beta (20–30 Hz) and the gamma (30–90 Hz) bands.

LFP spectra were computed on 1-s non overlapping windows. We used the multi-taper method of Thomson (Mitra and Pesaran, 1999; Pesaran et al., 2002) provided in the chronux package (Chronux.org). This method provides a trade-off between minimizing the variance of the power spectral estimate and maximizing the spectro-temporal resolution. The tapers used here are a family of orthogonal tapers and are given by the Slepian functions. They are parameterized by their length in time (T) and their bandwidth in Frequency. For the $T = 1$-s windows of data used here, a bandwidth of 2 Hz was attained by using three Slepian data tapers. The 60 Hz noise was removed and the power spectra were extrapolated around this frequency.

4.7.4. Theta–gamma phase amplitude coupling (PAC)

PAC was quantified using an estimate of the modulation index (MI; Tort et al., 2010), which is described in detail (Dvorak and Fenton, 2014). First, LFP signals were band-pass filtered (FIR filters, 2 Hz pass-band) in the slow frequency range and the instantaneous phase was extracted using the Hilbert transform (Fig 1D middle, left). LFP signals were also band-pass filtered in the fast frequency range (FIR filters, 20 Hz pass-band) and the instantaneous amplitude was extracted using the Hilbert transform (Fig. 1D bottom, left). Second, the phase–amplitude distribution was computed by extracting the mean amplitudes for each corresponding phase bin (Fig. 1D top, right). Third, MI was estimated as a Kullback–Leibler divergence between the resulting phase-amplitude distribution and the uniform distribution. Fourth, the normalized MI was estimated as a z score computed from the null distribution resulting from MI computed from time-offset phase and amplitude time series. Repeating the above steps for a series of frequencies for both slow and fast frequency ranges results in a comodulogram (Fig. 1D bottom, right). Inspection of the comodulograms revealed clear theta (7–8 Hz) phase modulation of gamma (30–100 Hz) oscillation amplitudes. Accordingly, analyses were focused on theta–gamma coupling. Numerical analyses examined the peak frequency of the theta modulating oscillations, as well as the peak frequency of the modulated gamma oscillations. The theta- and gamma band frequencies at the peak of each comodulogram were used to define the MI for statistical comparisons. We also estimated the average MI during 10-min time periods within each behavioral session. Note that the theta phase and gamma amplitude estimates for computing PAC were made from the same, local electrode instead of selecting a single site for estimating theta. Nonetheless, we also computed PAC at each electrode site using theta at sp and confirmed that the two PAC estimates were strongly correlated ($r = 0.90$; $P = 10^{-80}$), since theta is coherent across these hippocampal sites (Royer et al., 2010; Patel et al., 2012).

The pattern of theta–gamma PAC across multiple recording sites was quantified as an oscillatory activity vector by computing for each site the average modulation index (MI) at the peak of the theta–gamma comodulation (e.g. the value at the white + in the upper left comodulogram in Fig. 3A). The set of these MI values comprised the activity vector. To assess how the pattern of theta–gamma comodulation changes, pairs of activity vectors were correlated or their Euclidean distance was computed.

4.7.5. Debiased weighted phase lag index-square estimator (dWPLI)

The working hypothesis assumes that CA1 inputs from hippocampus CA3 and entorhinal cortex carry different information that requires coordination. We evaluated this assumption within the LFP data set by computing the debiased weighted phase lag index-square estimator (dWPLI) to estimate the frequency-specific coordination of neural activity between electrode pairs from the sp, sr, and slm recording sites. dWPLI was selected over the phase-locking value (Lachaux et al., 1999) to estimate phase synchrony because dWPLI minimizes the influence of volume conduction and is robust to small sample size, although it is unable to estimate delta phase synchrony because delta in our samples are nearly in phase (Vinck et al., 2011). Stronger phase synchrony was predicted between the input and output site pairs (sr and sp; slm and sp), than between the input sites sr and slm, on the assumption that sr and slm represent independent information streams. The dWPLI at a pair of electrodes was computed according to a published algorithm (Vinck et al., 2011). WPLI is based solely on the imaginary component of the cross-spectrum. The cross-spectra were computed on 3-s non-overlapping windows using the multi-taper method of Thomson, as described for Power Spectra above (Mitra and Pesaran, 1999; Pesaran et al., 2002). For the $T = 3$-s windows of data used here, a bandwidth of 2 Hz was attained by using three Slepian data tapers. WPLI was computed according to Eq. (1).

$$WPLI = \frac{E\{\mathfrak{I}\{X\}\}}{E\{|\mathfrak{I}\{X\}|\}} \tag{1}$$

where X is the cross-spectrum of signals coming from a pair of electrodes, E is the mean, $\mathfrak{I}\{X\}$ is the imaginary component of the cross-spectrum and $|\mathfrak{I}[X]|$ is its magnitude. We used the debiased weighted phase lag index (dWPLI) WPLI-squared estimator, which removes the positive bias in the estimation process according to Eq. (2) (Vinck et al., 2010).

$$\text{debiased WPLI} = \frac{E\{\mathfrak{I}\{X\}\}^2 - E\left\{\mathfrak{I}\{X\}^2\right\}}{E\{|\mathfrak{I}\{X\}|\}^2 - E\left\{\mathfrak{I}\{X\}^2\right\}} \tag{2}$$

4.7.6. Statistics

Statistical evaluation relied on parametric statistics because the data sets were approximately normally distributed. Statistical comparisons to investigate the effects of genotype and training session were made using two-way repeated measures ANOVA, or ANCOVA with speed as a covariate, when changes in locomotor speed could influence outcomes such as PAC magnitude. On the assumption that there might also be effects of within-session learning, the session data were subdivided into three 10-min epochs and the effects of genotype, training session, and epoch were examined by three-way repeated measures ANOVA or ANCOVA, with speed as the covariate. Specific planned comparisons such as the effect of introducing shock for the first time, or of 24-h retention, or of changing the shock zone on conflict or extinction training sessions, were performed by paired comparisons between the same time periods of two session types (e.g. last 10 min of pretraining versus training; last 10 min of final training session versus last 10 min of retention; last 10 min of retention versus last 10 min of conflict or extinction). These comparisons were made by two-way genotype and session type repeated measures ANCOVA, with speed as the covariate. Statistical significance was accepted for $P < 0.05$ with Bonferroni corrections of alpha as necessary. Post-hoc tests were performed using Tukey comparisons.

Author contributions

DD and AAF created software and hardware for data collection, BR collected data, BR and DD analyzed data and created figures, AAF designed and supervised research and wrote the manuscript.

Competing interests

There are no competing interests.

Acknowledgments

This study is supported by the NIH grant R01MH099128.

Appendix A. Supplementary data

Supplementary data to this article can be found online at http://dx.doi.org/10.1016/j.nbd.2016.01.003.

References

Abdel Baki, S.G., Kao, H.Y., Kelemen, E., Fenton, A.A., Bergold, P.J., 2009. A hierarchy of neurobehavioral tasks discriminates between mild and moderate brain injury in rats. Brain Res. 1280, 98–106.

Agarwal, G., Stevenson, I.H., Berenyi, A., Mizuseki, K., Buzsaki, G., Sommer, F.T., 2014. Spatially distributed local fields in the hippocampus encode rat position. Science 344, 626–630.

Ahmed, O.J., Mehta, M.R., 2012. Running speed alters the frequency of hippocampal gamma oscillations. J. Neurosci. 32, 7373–7383.
Auerbach, B.D., Bear, M.F., 2010. Loss of the fragile X mental retardation protein decouples metabotropic glutamate receptor dependent priming of long-term potentiation from protein synthesis. J. Neurophysiol. 104, 1047–1051.
Bailey Jr., D.B., Mesibov, G.B., Hatton, D.D., Clark, R.D., Roberts, J.E., Mayhew, L., 1998. Autistic behavior in young boys with fragile X syndrome. J. Autism Dev. Disord. 28, 499–508.
Bakker, C.E., Oostra, B.A., 2003. Understanding fragile X syndrome: insights from animal models. Cytogenet. Genome. Res. 100, 111–123.
Bakker, C.E., Verheij, C., Willemsen, R., Vanderhelm, R., Oerlemans, F., Vermey, M., Bygrave, A., Hoogeveen, A.T., Oostra, B.A., Reyniers, E., DeBoulle, K., Dhooge, R., Cras, P., Van Velzen, N., Nagels, G., Martin, J.J., Dedeyn, P.P., Darby, J.K., Willems, P.J., 1994. Fmr1 knockout mice: a model to study fragile X mental retardation. The Fragile X Consortium. Cell 78, 23–33.
Bassell, G.J., Warren, S.T., 2008. Fragile X syndrome: loss of local mRNA regulation alters synaptic development and function. Neuron 60, 201–214.
Bear, M.F., Huber, K.M., Warren, S.T., 2004. The mGluR theory of fragile X mental retardation. Trends Neurosci. 27, 370–377.
Berry-Kravis, E.M., Hessl, D., Rathmell, B., Zarevics, P., Cherubini, M., Walton-Bowen, K., Mu, Y., Nguyen, D.V., Gonzalez-Heydrich, J., Wang, P.P., Carpenter, R.L., Bear, M.F., Hagerman, R.J., 2012. Effects of STX209 (arbaclofen) on neurobehavioral function in children and adults with fragile X syndrome: a randomized, controlled, phase 2 trial. Sci. Transl. Med. 4 152ra127.
Bhakar, A.L., Dolen, G., Bear, M.F., 2012. The pathophysiology of fragile X (and what it teaches us about synapses). Annu. Rev. Neurosci. 35, 417–443.
Bhattacharya, A., Kaphzan, H., Alvarez-Dieppa, A.C., Murphy, J.P., Pierre, P., Klann, E., 2012. Genetic removal of p70 S6 kinase 1 corrects molecular, synaptic, and behavioral phenotypes in fragile X syndrome mice. Neuron 76, 325–337.
Bieri, K.W., Bobbitt, K.N., Colgin, L.L., 2014. Slow and fast gamma rhythms coordinate different spatial coding modes in hippocampal place cells. Neuron 82, 670–681.
Bragin, A., Jando, G., Nadasdy, Z., Hetke, J., Wise, K., Buzsaki, G., 1995. Gamma (40–100 Hz) oscillation in the hippocampus of the behaving rat. J. Neurosci. 15, 47–60.
Braun, K., Segal, M., 2000. FMRP involvement in formation of synapses among cultured hippocampal neurons. Cereb. Cortex 10, 1045–1052.
Brennan, F.X., Albeck, D.S., Paylor, R., 2006. Fmr1 knockout mice are impaired in a leverpress escape/avoidance task. Genes Brain Behav. 5, 467–471.
Burghardt, N.S., Park, E.H., Hen, R., Fenton, A.A., 2012. Adult-born hippocampal neurons promote cognitive flexibility in mice. Hippocampus 22, 1795–1808.
Buzsaki, G., 2010. Neural syntax: cell assemblies, synapsembles, and readers. Neuron 68, 362–385.
Buzsaki, G., Leung, L.W., Vanderwolf, C.H., 1983. Cellular bases of hippocampal EEG in the behaving rat. Brain Res. 287, 139–171.
Buzsaki, G., Buhl, D.L., Harris, K.D., Csicsvari, J., Czeh, B., Morozov, A., 2003. Hippocampal network patterns of activity in the mouse. Neuroscience 116, 201–211.
Buzsaki, G., Anastassiou, C.A., Koch, C., 2012. The origin of extracellular fields and currents–EEG, ECoG, LFP and spikes. Nat. Rev. Neurosci. 13, 407–420.
Canolty, R.T., Edwards, E., Dalal, S.S., Soltani, M., Nagarajan, S.S., Kirsch, H.E., Berger, M.S., Barbaro, N.M., Knight, R.T., 2006. High gamma power is phase-locked to theta oscillations in human neocortex. Science 313, 1626–1628.
Chen, Z., Resnik, E., McFarland, J.M., Sakmann, B., Mehta, M.R., 2011. Speed controls the amplitude and timing of the hippocampal gamma rhythm. PLoS ONE 6, e21408.
Chen, T., Lu, J.S., Song, Q., Liu, M.G., Koga, K., Descalzi, G., Li, Y.Q., Zhuo, M., 2014. Pharmacological rescue of cortical synaptic and network potentiation in a mouse model for fragile X syndrome. Neuropsychopharmacology 39, 1955–1967.
Cimadevilla, J.M., Wesierska, M., Fenton, A.A., Bures, J., 2001. Inactivating one hippocampus impairs avoidance of a stable room-defined place during dissociation of arena cues from room cues by rotation of the arena. Proc. Natl. Acad. Sci. U. S. A. 98, 3531–3536.
Colak, D., Zaninovic, N., Cohen, M.S., Rosenwaks, Z., Yang, W.-Y., Gerhardt, J., Disney, M.D., Jaffrey, S.R., 2014. Promoter-bound trinucleotide repeat mRNA drives epigenetic silencing in fragile X syndrome. Science 343, 1002–1005.
Colgin, L.L., Denninger, T., Fyhn, M., Hafting, T., Bonnevie, T., Jensen, O., Moser, M.B., Moser, E.I., 2009. Frequency of gamma oscillations routes flow of information in the hippocampus. Nature 462, 353–357.
Comery, T.A., Harris, J.B., Willems, P.J., Oostra, B.A., Irwin, S.A., Weiler, I.J., Greenough, W.T., 1997. Abnormal dendritic spines in fragile X knockout mice: maturation and pruning deficits. Proc. Natl. Acad. Sci. U. S. A. 94, 5401–5404.
Csicsvari, J., Jamieson, B., Wise, K.D., Buzsaki, G., 2003a. Mechanisms of gamma oscillations in the hippocampus of the behaving rat. Neuron 37, 311–322.
Csicsvari, J., Henze, D.A., Jamieson, B., Harris, K.D., Sirota, A., Bartho, P., Wise, K.D., Buzsaki, G., 2003b. Massively parallel recording of unit and local field potentials with silicon-based electrodes. J. Neurophysiol. 90, 1314–1323.
Deng, P.Y., Sojka, D., Klyachko, V.A., 2011. Abnormal presynaptic short-term plasticity and information processing in a mouse model of fragile X syndrome. J. Neurosci. 31, 10971–10982.
D'Hooge, R., Nagels, G., Franck, F., Bakker, C.E., Reyniers, E., Storm, K., Kooy, R.F., Oostra, B.A., Willems, P.J., De Deyn, P.P., 1997. Mildly impaired water maze performance in male Fmr1 knockout mice. Neuroscience 76, 367–376.
Dolen, G., Osterweil, E., Rao, B.S., Smith, G.B., Auerbach, B.D., Chattarji, S., Bear, M.F., 2007. Correction of fragile X syndrome in mice. Neuron 56, 955–962.
Dvorak, D., Fenton, A.A., 2014. Toward a proper estimation of phase–amplitude coupling in neural oscillations. J. Neurosci. Methods 225C, 42–56.
Eadie, B.D., Cushman, J., Kannangara, T.S., Fanselow, M.S., Christie, B.R., 2012. NMDA receptor hypofunction in the dentate gyrus and impaired context discrimination in adult Fmr1 knockout mice. Hippocampus 22, 241–254.
Erickson, C.A., Veenstra-Vanderweele, J.M., Melmed, R.D., McCracken, J.T., Ginsberg, L.D., Sikich, L., Scahill, L., Cherubini, M., Zarevics, P., Walton-Bowen, K., Carpenter, R.L., Bear, M.F., Wang, P.P., King, B.H., 2013. STX209 (arbaclofen) for autism spectrum disorders: an 8-week open-label study. J. Autism Dev. Disord. 44, 958–964.
Fenton, A.A., 2008. Neural Coordination and Psychotic Disorganization In: Information Processing by Neuronal Populations (Holscher C, Munk MH, eds), pp 387–408. Cambridge University Press, London.
Fenton, A.A., 2015. Excitation–inhibition discoordination in rodent models of mental disorders. Biol. Psychiatry.
Fenton, A.A., Wesierska, M., Kaminsky, Y., Bures, J., 1998. Both here and there: simultaneous expression of autonomous spatial memories in rats. Proc. Natl. Acad. Sci. U. S. A. 95, 11493–11498.
Fenton, A.A., Lytton, W.W., Barry, J.M., Lenck-Santini, P.P., Zinyuk, L.E., Kubik, S., Bures, J., Poucet, B., Muller, R.U., Olypher, A.V., 2010. Attention-like modulation of hippocampus place cell discharge. J. Neurosci. 30, 4613–4625.
Fries, P., 2009. The model- and the data-gamma. Neuron 64, 601–602.
Godfraind, J.M., Reyniers, E., De Boulle, K., D'Hooge, R., De Deyn, P.P., Bakker, C.E., Oostra, B.A., Kooy, R.F., Willems, P.J., 1996. Long-term potentiation in the hippocampus of fragile X knockout mice. Am. J. Med. Genet. 64, 246–251.
Gothard, K.M., Skaggs, W.E., McNaughton, B.L., 1996. Dynamics of mismatch correction in the hippocampal ensemble code for space: interaction between path integration and environmental cues. J. Neurosci. 16, 8027–8040.
Hagerman, R., Hoem, G., Hagerman, P., 2010. Fragile X and autism: intertwined at the molecular level leading to targeted treatments. Mol. Autism. 1, 12.
Holsen, L.M., Dalton, K.M., Johnstone, T., Davidson, R.J., 2008. Prefrontal social cognition network dysfunction underlying face encoding and social anxiety in fragile X syndrome. NeuroImage 43, 592–604.
Hooper, S.R., Hatton, D., Sideris, J., Sullivan, K., Hammer, J., Schaaf, J., Mirrett, P., Ornstein, P.A., Bailey Jr., D.P., 2008. Executive functions in young males with fragile X syndrome in comparison to mental age-matched controls: baseline findings from a longitudinal study. Neuropsychology 22, 36–47.
Huber, K.M., Gallagher, S.M., Warren, S.T., Bear, M.F., 2002. Altered synaptic plasticity in a mouse model of fragile X mental retardation. Proc. Natl. Acad. Sci. U. S. A. 99, 7746–7750.
Jin, P., Zarnescu, D.C., Ceman, S., Nakamoto, M., Mowrey, J., Jongens, T.A., Nelson, D.L., Moses, K., Warren, S.T., 2004. Biochemical and genetic interaction between the fragile X mental retardation protein and the microRNA pathway. Nat. Neurosci. 7, 113–117.
Johnson, A., Redish, A.D., 2007. Neural ensembles in CA3 transiently encode paths forward of the animal at a decision point. J. Neurosci. 27, 12176–12189.
Kao, D.I., Aldridge, G.M., Weiler, I.J., Greenough, W.T., 2010. Altered mRNA transport, docking, and protein translation in neurons lacking fragile X mental retardation protein. Proc. Natl. Acad. Sci. U. S. A. 107, 15601–15606.
Kelemen, E., Fenton, A.A., 2010. Dynamic grouping of hippocampal neural activity during cognitive control of two spatial frames. PLoS Biol. 8, e1000403.
Kelemen, E., Fenton, A.A., 2013. Key features of human episodic recollection in the cross-episode retrieval of rat hippocampus representations of space. PLoS Biol. 11, e1001607.
Kheirbek, M.A., Drew, L.J., Burghardt, N.S., Costantini, D.O., Tannenholz, L., Ahmari, S.E., Zeng, H., Fenton, A.A., Hen, R., 2013. Differential control of learning and anxiety along the dorsoventral axis of the dentate gyrus. Neuron 77, 955–968.
Kiss, J., Buzsaki, G., Morrow, J.S., Glantz, S.B., Leranth, C., 1996. Entorhinal cortical innervation of parvalbumin-containing neurons (basket and chandelier cells) in the rat Ammon's horn. Hippocampus 6, 239–246.
Klausberger, T., Magill, P.J., Marton, L.F., Roberts, J.D., Cobden, P.M., Buzsaki, G., Somogyi, P., 2003. Brain-state- and cell-type-specific firing of hippocampal interneurons in vivo. Nature 421, 844–848.
Kramer, M.A., Tort, A.B., Kopell, N.J., 2008. Sharp edge artifacts and spurious coupling in EEG frequency comodulation measures. J. Neurosci. Methods 170, 352–357.
Krueger, D.D., Osterweil, E.K., Chen, S.P., Tye, L.D., Bear, M.F., 2011. Cognitive dysfunction and prefrontal synaptic abnormalities in a mouse model of fragile X syndrome. Proc. Natl. Acad. Sci. U. S. A. 108, 2587–2592.
Kubik, S., Fenton, A.A., 2005. Behavioral evidence that segregation and representation are dissociable hippocampal functions. J. Neurosci. 25, 9205–9212.
Lachaux, J.P., Rodriguez, E., Martinerie, J., Varela, F.J., 1999. Measuring phase synchrony in brain signals. Hum. Brain Mapp. 8, 194–208.
Lakatos, P., Shah, A.S., Knuth, K.H., Ulbert, I., Karmos, G., Schroeder, C.E., 2005. An oscillatory hierarchy controlling neuronal excitability and stimulus processing in the auditory cortex. J. Neurophysiol. 94, 1904–1911.
Smoller JWC-DGotPGC, 2013. Identification of risk loci with shared effects on five major psychiatric disorders: a genome-wide analysis. Lancet 381, 1371–1379.
Larson, J., Jessen, R.E., Kim, D., Fine, A.K., du Hoffmann, J., 2005. Age-dependent and selective impairment of long-term potentiation in the anterior piriform cortex of mice lacking the fragile X mental retardation protein. J. Neurosci. 25, 9460–9469.
Lasztoczi, B., Klausberger, T., 2014. Layer-specific GABAergic control of distinct gamma oscillations in the CA1 hippocampus. Neuron 81, 1126–1139.
Lauterborn, J.C., Rex, C.S., Kramar, E., Chen, L.Y., Pandyarajan, V., Lynch, G., Gall, C.M., 2007. Brain-derived neurotrophic factor rescues synaptic plasticity in a mouse model of fragile X syndrome. J. Neurosci. 27, 10685–10694.
Lee, H., Dvorak, D., Kao, H.Y., Duffy, A.M., Scharfman, H.E., Fenton, A.A., 2012. Early cognitive experience prevents adult deficits in a neurodevelopmental schizophrenia model. Neuron 75, 714–724.
Lee, H., Dvorak, D., Fenton, A.A., 2014. Targeting neural synchrony deficits is sufficient to improve cognition in a schizophrenia-related neurodevelopmental model. Front Psychiat. 5, 15.
Lisman, J., Buzsaki, G., 2008. A neural coding scheme formed by the combined function of gamma and theta oscillations. Schizophr. Bull. 34, 974–980.

Lisman, J.E., Jensen, O., 2013. The theta–gamma neural code. Neuron 77, 1002–1016.
Markram, H., Rinaldi, T., Markram, K., 2007. The intense world syndrome—an alternative hypothesis for autism. Front. Neurosci. 1, 77–96.
McFarland, W.L., Teitelbaum, H., Hedges, E.K., 1975. Relationship between hippocampal theta activity and running speed in the rat. J. Comp. Physiol. Psychol. 88, 324–328.
Melko, M., Bardoni, B., 2010. The role of G-quadruplex in RNA metabolism: involvement of FMRP and FMR2P. Biochimie 92, 919–926.
Mitchell KJ, O'Donnell P, Durstewitz D, Fenton AA, Gingrich JA, Gordon JA, Kelsch W, Moghaddam B, Phillips WA, Sawa A (2013) A framework for the use of models in schizophrenia. In: Schizophrenia: Evolution and Synthesis (Silverstein SM, Moghaddam B, Wykes T, eds), pp 212–226. Cambridge, MA: MIT Press.
Mitra, P.P., Pesaran, B., 1999. Analysis of dynamic brain imaging data. Biophys. J. 76, 691–708.
Montgomery, S.M., Buzsaki, G., 2007. Gamma oscillations dynamically couple hippocampal CA3 and CA1 regions during memory task performance. Proc. Natl. Acad. Sci. U. S. A. 104, 14495–14500.
Montgomery, S.M., Betancur, M.I., Buzsaki, G., 2009. Behavior-dependent coordination of multiple theta dipoles in the hippocampus. J. Neurosci. 29, 1381–1394.
Moon, J., Beaudin, A.E., Verosky, S., Driscoll, L.L., Weiskopf, M., Levitsky, D.A., Crnic, L.S., Strupp, B.J., 2006. Attentional dysfunction, impulsivity, and resistance to change in a mouse model of fragile X syndrome. Behav. Neurosci. 120, 1367–1379.
Moon, J., Ota, K.T., Driscoll, L.L., Levitsky, D.A., Strupp, B.J., 2008. A mouse model of fragile X syndrome exhibits heightened arousal and/or emotion following errors or reversal of contingencies. Dev. Psychobiol. 50, 473–485.
Moreno, H., Burghardt, N.S., Vela-Duarte, D., Masciotti, J., Hua, F., Fenton, A.A., Schwaller, B., Small, S.A., 2011. The absence of the calcium-buffering protein calbindin is associated with faster age-related decline in hippocampal metabolism. Hippocampus.
O'Keefe, J., Burgess, N., 1996. Geometric determinants of the place fields of hippocampal neurons. Nature 381, 425–428.
O'Reilly, K.C., Kao, H.-Y., Lee, H., Fenton, A.A., 2014. Converging on a core cognitive deficit: the impact of various neurodevelopment insults on cognitive control. Front. Neurosci. 8.
Ornstein, P.A., Schaaf, J.M., Hooper, S.R., Hatton, D.D., Mirrett, P., Bailey Jr., D.B., 2008. Memory skills of boys with fragile X syndrome. Am. J. Ment. Retard. 113, 453–465.
Osterweil, E.K., Chuang, S.C., Chubykin, A.A., Sidorov, M., Bianchi, R., Wong, R.K., Bear, M.F., 2013. Lovastatin corrects excess protein synthesis and prevents epileptogenesis in a mouse model of fragile X syndrome. Neuron 77, 243–250.
Papp, E., Leinekugel, X., Henze, D.A., Lee, J., Buzsaki, G., 2001. The apical shaft of CA1 pyramidal cells is under GABAergic interneuronal control. Neuroscience 102, 715–721.
Park, S., Park, J.M., Kim, S., Kim, J.A., Shepherd, J.D., Smith-Hicks, C.L., Chowdhury, S., Kaufmann, W., Kuhl, D., Ryazanov, A.G., Huganir, R.L., Linden, D.J., Worley, P.F., 2008. Elongation factor 2 and fragile X mental retardation protein control the dynamic translation of Arc/Arg3.1 essential for mGluR-LTD. Neuron 59, 70–83.
Park, E.H., Burghardt, N.S., Dvorak, D., Hen, R., Fenton, A.A., 2015. Experience-dependent regulation of dentate gyrus excitability by adult-born granule cells. J. Neurosci. 35, 11656–11666.
Pastalkova, E., Serrano, P., Pinkhasova, D., Wallace, E., Fenton, A.A., Sacktor, T.C., 2006. Storage of spatial information by the maintenance mechanism of LTP. Science 313, 1141–1144.
Pastalkova, E., Itskov, V., Amarasingham, A., Buzsaki, G., 2008. Internally generated cell assembly sequences in the rat hippocampus. Science 321, 1322–1327.
Patel, J., Fujisawa, S., Berenyi, A., Royer, S., Buzsaki, G., 2012. Traveling theta waves along the entire septotemporal axis of the hippocampus. Neuron 75, 410–417.
Penttonen, M., Kamondi, A., Acsady, L., Buzsaki, G., 1998. Gamma frequency oscillation in the hippocampus of the rat: intracellular analysis in vivo. Eur. J. Neurol. 10, 718–728.
Pesaran, B., Pezaris, J.S., Sahani, M., Mitra, P.P., Andersen, R.A., 2002. Temporal structure in neuronal activity during working memory in macaque parietal cortex. Nat. Neurosci. 5, 805–811.
Phillips, W.A., Silverstein, S.M., 2003. Convergence of biological and psychological perspectives on cognitive coordination in schizophrenia. Behav. Brain Sci. 26, 65–82 discussion 82-137.
Phillips, W.A., Singer, W., 1997. In search of common foundations for cortical computation. Behav. Brain Sci. 20, 657–683 discussion 683-722.
Pieretti, M., Zhang, F.P., Fu, Y.H., Warren, S.T., Oostra, B.A., Caskey, C.T., Nelson, D.L., 1991. Absence of expression of the FMR-1 gene in fragile X syndrome. Cell 66, 817–822.
Pollack, A., 2013. An Experimental Drug's Bitter End. In: New York Times, New York Edition Edition, p B1. New York Times Company, New York City.
Royer, S., Sirota, A., Patel, J., Buzsaki, G., 2010. Distinct representations and theta dynamics in dorsal and ventral hippocampus. J. Neurosci. 30, 1777–1787.
Sargolini, F., Fyhn, M., Hafting, T., McNaughton, B.L., Witter, M.P., Moser, M.B., Moser, E.I., 2006. Conjunctive representation of position, direction, and velocity in entorhinal cortex. Science 312, 758–762.
Sauseng, P., Klimesch, W., Heise, K.F., Gruber, W.R., Holz, E., Karim, A.A., Glennon, M., Gerloff, C., Birbaumer, N., Hummel, F.C., 2009. Brain oscillatory substrates of visual short-term memory capacity. Curr. Biol. 19, 1846–1852.
Savelli, F., Yoganarasimha, D., Knierim, J.J., 2008. Influence of boundary removal on the spatial representations of the medial entorhinal cortex. Hippocampus 18, 1270–1282.
Schomburg, E.W., Fernandez-Ruiz, A., Mizuseki, K., Berenyi, A., Anastassiou, C.A., Koch, C., Buzsaki, G., 2014. Theta phase segregation of input-specific gamma patterns in entorhinal-hippocampal networks. Neuron 84, 470–485.
Segal, M., Kreher, U., Greenberger, V., Braun, K., 2003. Is fragile X mental retardation protein involved in activity-induced plasticity of dendritic spines? Brain Res. 972, 9–15.
Shang, Y., Wang, H., Mercaldo, V., Li, X., Chen, T., Zhuo, M., 2009. Fragile X mental retardation protein is required for chemically-induced long-term potentiation of the hippocampus in adult mice. J. Neurochem. 111, 635–646.
Sharma, A., Hoeffer, C.A., Takayasu, Y., Miyawaki, T., McBride, S.M., Klann, E., Zukin, R.S., 2010. Dysregulation of mTOR signaling in fragile X syndrome. J. Neurosci. 30, 694–702.
Sidorov, M.S., Krueger, D.D., Taylor, M., Gisin, E., Osterweil, E.K., Bear, M.F., 2014. Extinction of an instrumental response: a cognitive behavioral assay in Fmr1 knockout mice. Genes Brain Behav.
Tamanini, F., Meijer, N., Verheij, C., Willems, P.J., Galjaard, H., Oostra, B.A., Hoogeveen, A.T., 1996. FMRP is associated to the ribosomes via RNA. Hum. Mol. Genet. 5, 809–813.
Till, S.M., Asiminas, A., Jackson, A.D., Katsanevaki, D., Barnes, S.A., Osterweil, E.K., Bear, M.F., Chattarji, S., Wood, E.R., Wyllie, D.J., Kind, P.C., 2015. Conserved hippocampal cellular pathophysiology but distinct behavioural deficits in a new rat model of FXS. Hum. Mol. Genet.
Tort, A.B., Kramer, M.A., Thorn, C., Gibson, D.J., Kubota, Y., Graybiel, A.M., Kopell, N.J., 2008. Dynamic cross-frequency couplings of local field potential oscillations in rat striatum and hippocampus during performance of a T-maze task. Proc. Natl. Acad. Sci. U. S. A. 105, 20517–20522.
Tort, A.B., Komorowski, R., Eichenbaum, H., Kopell, N., 2010. Measuring phase–amplitude coupling between neuronal oscillations of different frequencies. J. Neurophysiol. 104, 1195–1210.
Traub, R.D., Whittington, M.A., Colling, S.B., Buzsaki, G., Jefferys, J.G., 1996. Analysis of gamma rhythms in the rat hippocampus in vitro and in vivo. J. Physiol. 493 (Pt 2), 471–484.
Vanderklish, P.W., Edelman, G.M., 2005. Differential translation and fragile X syndrome. Genes Brain Behav. 4, 360–384.
Vanderwolf, C.H., 1969. Hippocampal electrical activity and voluntary movement in the rat. Electroencephalogr. Clin. Neurophysiol. 26, 407–418.
Vinck, M., van Wingerden, M., Womelsdorf, T., Fries, P., Pennartz, C.M., 2010. The pairwise phase consistency: a bias-free measure of rhythmic neuronal synchronization. NeuroImage 51, 112–122.
Vinck, M., Oostenveld, R., van Wingerden, M., Battaglia, F., Pennartz, C.M., 2011. An improved index of phase-synchronization for electrophysiological data in the presence of volume-conduction, noise and sample-size bias. NeuroImage 55, 1548–1565.
Wang, X.J., Buzsaki, G., 1996. Gamma oscillation by synaptic inhibition in a hippocampal interneuronal network model. J. Neurosci. 16, 6402–6413.
Wesierska, M., Dockery, C., Fenton, A.A., 2005. Beyond memory, navigation, and inhibition: behavioral evidence for hippocampus-dependent cognitive coordination in the rat. J. Neurosci. 25, 2413–2419.
Whittington, M.A., Traub, R.D., 2003. Interneuron diversity series: inhibitory interneurons and network oscillations in vitro. Trends Neurosci. 26, 676–682.
Whittington, M.A., Traub, R.D., Jefferys, J.G., 1995. Synchronized oscillations in interneuron networks driven by metabotropic glutamate receptor activation. Nature 373, 612–615.
Zhang, S.J., Ye, J., Miao, C., Tsao, A., Cerniauskas, I., Ledergerber, D., Moser, M.B., Moser, E.I., 2013. Optogenetic dissection of entorhinal-hippocampal functional connectivity. Science 340, 1232627.
Zhao, M.G., Toyoda, H., Ko, S.W., Ding, H.K., Wu, L.J., Zhuo, M., 2005. Deficits in trace fear memory and long-term potentiation in a mouse model for fragile X syndrome. J. Neurosci. 25, 7385–7392.
Zinyuk, L., Kubik, S., Kaminsky, Y., Fenton, A.A., Bures, J., 2000. Understanding hippocampal activity by using purposeful behavior: place navigation induces place cell discharge in both task-relevant and task-irrelevant spatial reference frames. Proc. Natl. Acad. Sci. U. S. A. 97, 3771–3776.